



# Failure Mechanism and Movement Characteristics of Overlying Strata in Longwall Mining Face with Thick Aquifer

Yuliang Wang<sup>1</sup> · Dezhong Kong<sup>2</sup> · Guiyi Wu<sup>3</sup> · Zhanbo Cheng<sup>4</sup> · Gaofeng Song<sup>5</sup> · Yuqi Shang<sup>3</sup>

Received: 1 November 2023 / Accepted: 20 April 2024 / Published online: 7 May 2024

© The Author(s), under exclusive licence to Springer-Verlag GmbH Austria, part of Springer Nature 2024

## Abstract

The failure and movement of overlying strata with a thick aquifer are closely related to the water-inrush pressure and the hydraulic coupling in coal mining faces. However, there is limited research on the large-scale failure mechanism and displacement law of overlying strata by considering fluid–solid coupling. In this study, taking Daojiao coal mine as an engineering background, the failure mechanism and movement characteristics of overlying strata with a thick aquifer are comprehensively investigated after considering fluid–solid coupling by means of theoretical analysis, large-scale physical simulation, and numerical simulation. The results show that seepage and water pressure can significantly affect the overlying strata-movement parameters that the initial and periodic breaking distances of the aquifuge under the action of hydraulic coupling increase with the increase of the tensile strength of rock, and the decrease of hydrostatic head. In addition, the overlying strata of thick aquifer can be regarded as tensile failure based on the simulation results. The overlying strata above the goaf generally sinks downward with a funnel shape, and the main roof periodically appears to be a cantilever-beam structure. Moreover, the periodic breaking distance of the aquifuge is about half of the initial breaking distance, which is consistent with the results of theoretical analysis.

## Highlights

- The expressions of the initial and periodic breaking distance of the aquifuge by considering hydraulic coupling are established.
- A large-scale physical simulation test of fluid-solid coupling under the combined action of water pressure and karst water seepage is designed.
- The numerical model of aquifer waterless mining and fluid-solid coupling mining are constructed.
- The failure mechanism and movement characteristics of overlying strata with a thick aquifer are expounded.

**Keywords** Thick aquifer · Failure mechanism · Hydrostatic pressure · Fluidsolid coupling

✉ Dezhong Kong  
dzkong@gzu.edu.cn

✉ Zhanbo Cheng  
zhanbo.cheng@ntu.edu.sg

Yuliang Wang  
15885190867@163.com

Guiyi Wu  
gywu@gzu.edu.cn

Gaofeng Song  
gaofeng.song@hotmail.com

Yuqi Shang  
gs.yqshang20@gzu.edu.cn

<sup>1</sup> School of Energy and Mining Engineering, China University of Mining and Technology (Beijing), Beijing 100083, China

<sup>2</sup> State Key Laboratory of Public Big Data, College of Mining, Guizhou Univ., Guiyang 550025, China

<sup>3</sup> College of Mining, Guizhou Univ., Guiyang 550025, China

<sup>4</sup> School of Engineering, University of Warwick, Coventry CV47AL, UK

<sup>5</sup> North China University of Technology, Beijing 100144, China

Rock	Rock type	Thickness	Total thickness	Lithological description
	Mudstone	10m	120m	Gray, soft texture, consolidation degree is weaker than shale, recrystallization is not obvious, easy to damage, horizontal joints, good water insulation.
	Limestone	50m	110m	The lithology is gray to dark gray medium-thick layered micro-to fine-grained limestone, bioclastic limestone, containing a small amount of black carbon mud and chert nodules ( or agglomerates ).
	Sandy mudstone	24m	60m	Deep gray, loose, easy to destroy, loose and fragile, horizontal joints, good water absorption.
	Mudstone	4m	36m	Gray, soft texture, weaker consolidation than shale, recrystallization is not obvious, easy to destroy, horizontal joints, good water resistance
	Sandy mudstone	4.5m	32m	Deep gray, loose, easy to destroy, loose and fragile, horizontal joints, good water absorption.
	Carbon mudstone	2.5m	27.5m	Organic carbon content of about 6-40%, coal measures strata between general mudstone and coal lithology.
	C3 coal seam	2m	25m	Black, containing brachiopods, plant fossils, coal layer and stable thickness, single structure, local containing a layer of dirt band
	Tonstein	10m	23m	The minerals are very small, and the crystal size does not exceed 1-2 microns. The main components are kaolinite, hydromica, montmorillonite, chlorite, etc.
	C1 coal seam	1m	13m	Black, containing brachiopods, plant fossils, single structure, partly containing a layer of dirt band
	Mudstone	12m	12m	Gray, soft texture, weaker consolidation than shale, recrystallization is not obvious, easy to destroy, horizontal joints, good water resistance

Fig. 1 Comprehensive histogram of rock formation

## 1 Introduction

The failure and movement of overlying strata under aquifer mining can lead to environmental and disaster problems such as groundwater loss, ground subsidence, and roof water inrush (Zhang et al. 2010; Miao et al 2011; Huang et al 2018; Kong et al. 2021a, 2021b). Especially, mine-water inrush, one of the five major disasters in coal mines, can submerge workfaces and roadways, seriously threatening the safe production of mining faces (Li et al. 2019, 2022; Wu et al. 2021). When coal mining was carried out under the condition of aquifer overburden, the aquiclude was easily destroyed under the combined action of mine pressure and pore-water pressure, which made the water-conducting fractures penetrate into the aquifer, resulting in the occurrence of mine-water-inrush disaster and the loss of water resources (Wang et al. 2021a, 2022). In addition, the thick aquifer can be further compressed and consolidated after water loss, accelerating the roof failure and surface subsidence process. After the end of mining, it is necessary to consider the impact of water on the closed mine because the

mining activities caused water-conducting fractures can connect groundwater or the surface, and the water may seep into the closed mine. The coal mine may suffer from flooding and groundwater pollution after closure (Zhang et al. 2020; Manzano et al. 1999; Gee et al. 2020; Manhong et al.2021). Therefore, it is of great significance to master the failure mechanism and movement characteristics of overlying strata with a thick aquifer for preventing and controlling coal-mine water damage, surface subsidence and ecological damage. Meanwhile, it is also beneficial to improve the early-warning capability of potential coal mine-water disasters, and achieve more effective coal mine-water disaster management and emergency response.

In recent years, there were plenty of researches on the rock mechanics behavior and rock-stability control (Song et al. 2023; Feng et al. 2020; Kong et al.2021c; Shang et al. 2022). Among them, based on the triaxial compression test of rough jointed rock, scholars have proposed a novel semi-empirical mathematical model to evaluate the equivalent dynamic shear strength (EDSS) of rock joints and a semi-empirical model to more rigorously quantify the critical

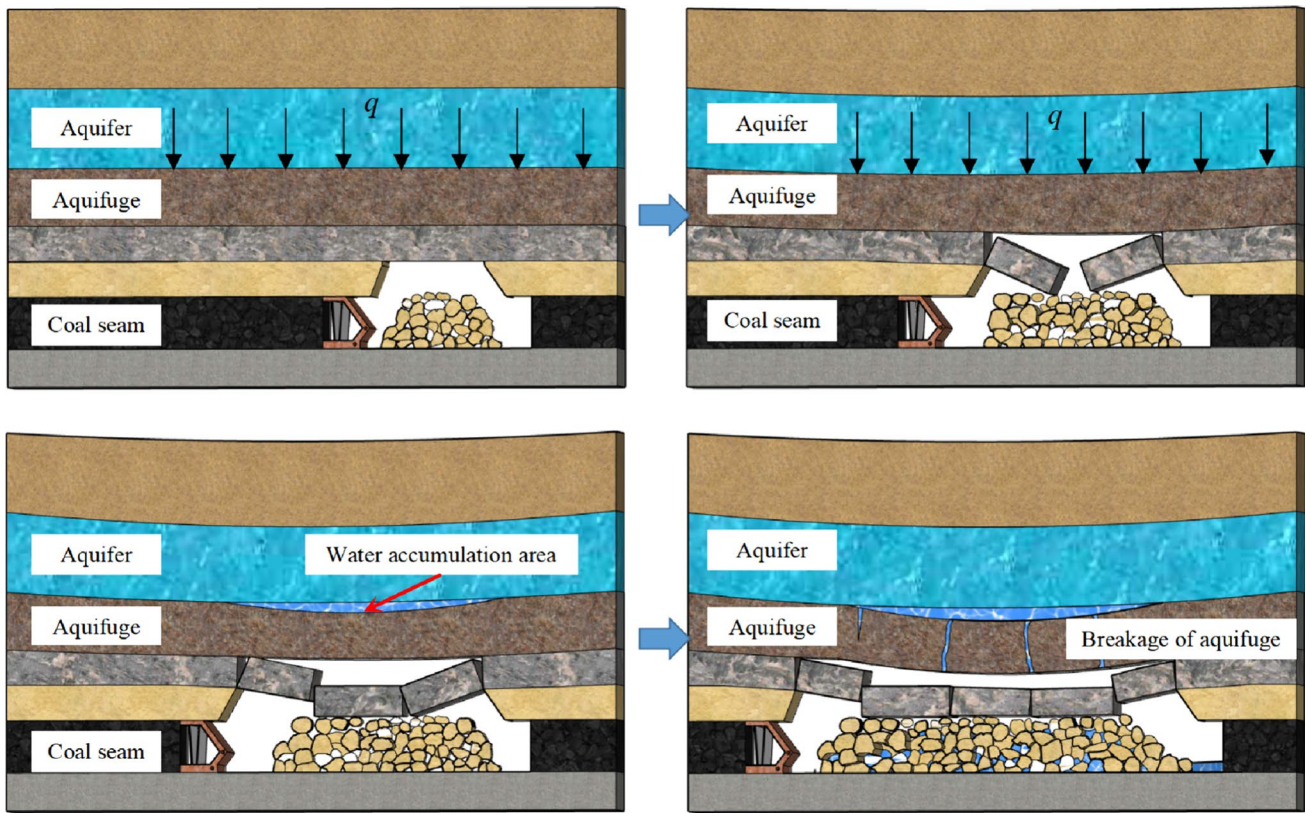


Fig. 2 Schematic diagram of the deformation and destruction process of the overlying strata during the mining process

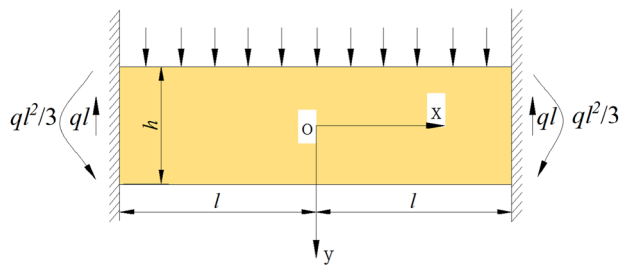
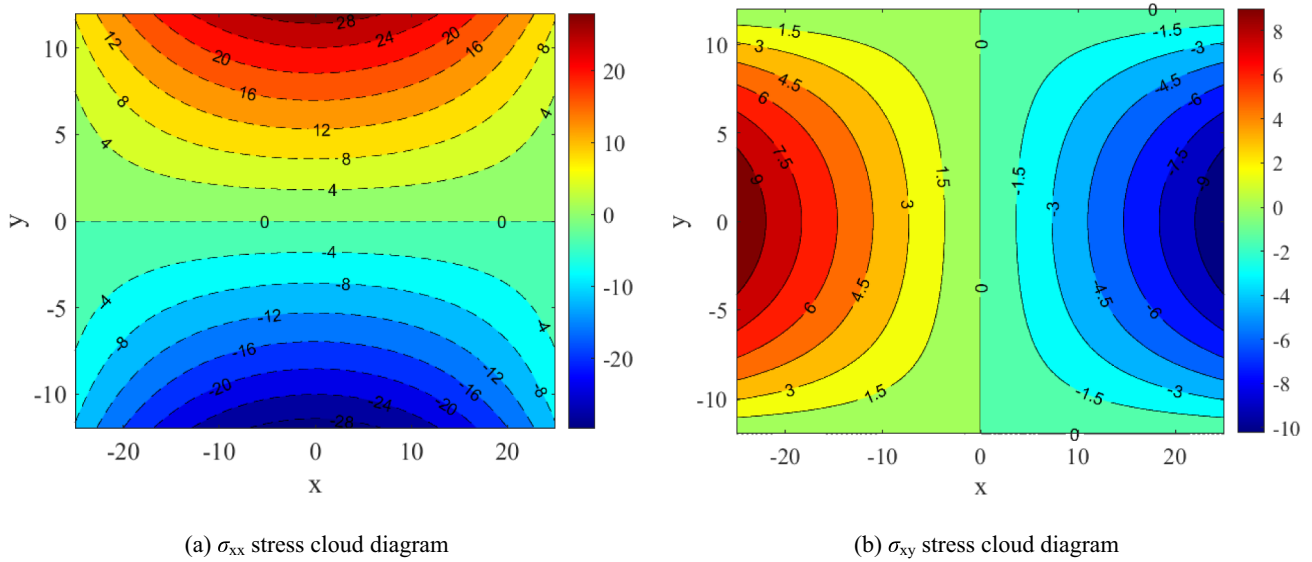


Fig. 3 Mechanical model analysis of clamped beam, where  $q$  is the load on the beam,  $\text{kN/m}$ ;  $h$  is the thickness of the beam,  $\text{m}$ ;  $l$  is the length from the midpoint to the endpoint of the beam,  $\text{m}$

shear strain ( $\epsilon_{\text{critical}}$ ) of rock joints, which lays a foundation for the study of overlying strata failure characteristics and movement rules (Buddhima et al. 2021; Mairaj et al. 2022; Pathan et al. 2022), which lays a foundation for the study of overlying strata failure characteristics and movement rules. However, there are relatively few studies on the failure and movement of overlying strata under aquifers. For this reason, relevant scholars have gradually focused on the study of the failure and movement law of overlying strata under aquifer mining. Liu and Elsworth (1997) proposed a coupling model between strain and hydraulic conductivity to evaluate the

increment of hydraulic conductivity and saturation of overlying strata around the longwall face. Zhang and Shen (2003) summarized the current situation of coal mining under aquifers in China, and evaluated the stress redistribution, strata failure and hydraulic conductivity enhancement of coal mining under water-bearing alluvium by means of field investigation, physical simulation and numerical analysis. Yang et al. (2007) presented a fully coupled flow–stress–damage model to simulate the progressive development of fractures and the associated groundwater flow under incremental loading conditions resulting from mining processes. The model is based on classical theories of porous media flow and damage mechanics and importantly links changes in permeability with the accumulation of damage in following the complete stress–strain process. Zhang et al. (2010) discussed the mechanism and basic requirements of the aquifer protection in longwall mining and the relationship between the fall of the water table and the surface subsidence. Fan and Zhang (2015) illustrated that the key strata played a dominant role in the deformation and fracture development of the overlying strata. In addition, the thickness of the interlayer affects the mining disturbance intensity of the aquifer, and it can be a protective layer to prevent water loss in the aquifer. Wang et al. (2015) studied the surface movement, failure characteristics of the overlying strata,



**Fig. 4** Stress cloud diagram of  $\sigma_{xx}$  and  $\sigma_{xy}$  of fixed beam structure in the aquifuge. **a**  $\sigma_{xx}$  stress cloud diagram. **b**  $\sigma_{xy}$  stress cloud diagram

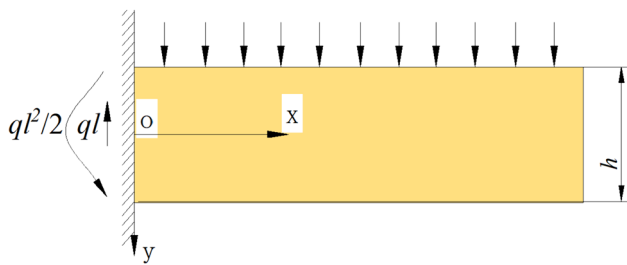


**Fig. 5** Mechanical model of the cantilever beam

and water percolation caused by coal mining under rivers by combining field monitoring, physical simulation and discrete element numerical simulation. Meng et al. (2012, 2016) and Zhao et al. (2022) illustrated that aquifers' impermeability and water pressure resistance varied with lithology and structural characteristics. Sun et al. (2017) analyzed the stress distribution, fracture characteristics, and water-inrush damaged area of water-resistant key strata using the elastic thin plate theory, which can further determine the maximum water pressure of bearing water-resistant key strata. Zhang

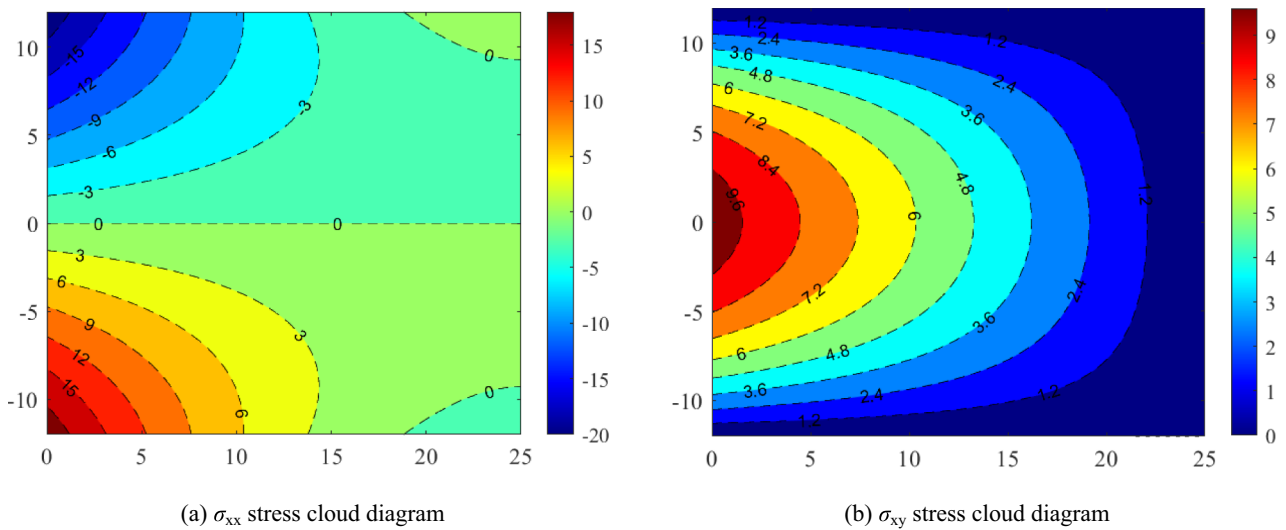
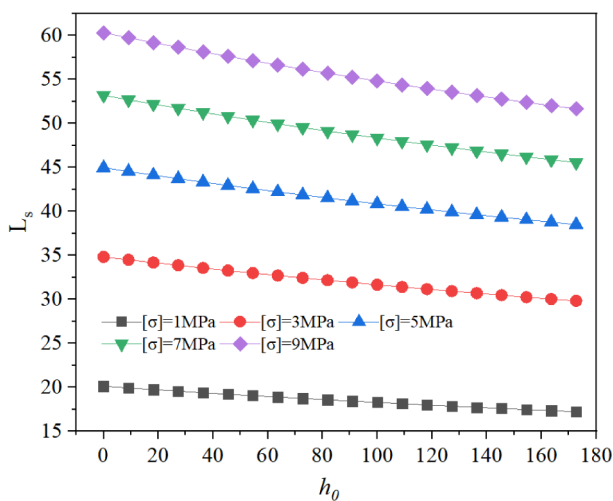
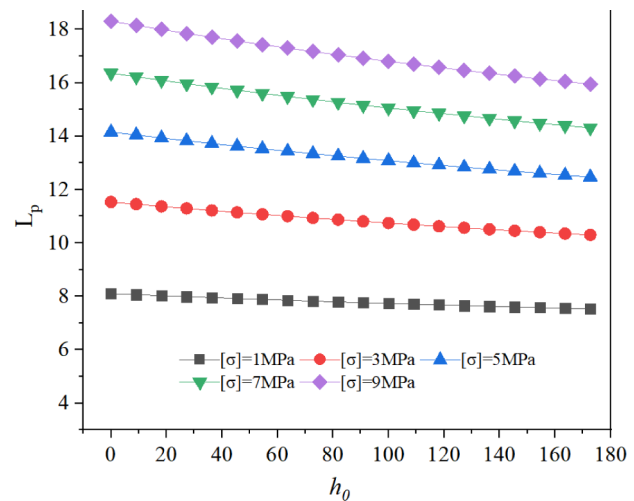


**Fig. 6**  $\sigma_{xx}$  and  $\sigma_{xy}$  stress distribution of aquifuge cantilever-beam structure. **a**  $\sigma_{xx}$  stress cloud diagram. **b**  $\sigma_{xy}$  stress cloud diagram





(a) Initial breaking distance



(b) Periodic breaking distance

**Fig. 7** Variation law of fracture distance of aquiclude with hydrostatic head and tensile strength of rock. **a** Initial breaking distance. **b** Periodic breaking distance

et al. (2019) studied the behavior of movement of overlying strata, water-level change, and groundwater inrush by An integrated method including borehole and working face observation, in-site water leakage, and real-time video imaging. Chen et al. (2019) established a modified Winkler elastic foundation beam model to calculate the height of water flowing fractured zone by considering the coupling effect of seawater pressure and backfill support. Many control measurements were proposed to protect the aquifer, such as the rapid advance of longwall face, reducing mining height, backfilling and grouting (Zhang and Shen 2003; Zhang and Peng 2005; Zhang et al. 2010). Moreover, the numerical simulation was commonly adopted to study the mechanism of mine-water inrush caused by mining activities (Rui et al. 2018; Huang et al. 2021; Fan et al. 2021; Wang et al. 2022; Chen et al. 2022). For example, FLAC3D has been widely used to study the development characteristics of the fracture zone above the goaf, the fracture characteristics of the overlying strata, the movement law of the overlying strata, and the surface subsidence. (Wang et al. 2021b; Sikora and Wesołowski 2021; Niu et al. 2022; Ding et al. 2022).

Throughout the literature review, several key issues in the mining process of coal seam under aquifer conditions, including stress distribution, protection mechanisms, development of water-conducting fractures and the relationship between water-level decline and surface subsidence, were comprehensively studied through theoretical analysis, physical simulation, and numerical simulation. However, there are relatively few studies on the failure mechanism and movement characteristics of overlying strata under the hydro-mechanical coupling in thick aquifers. In addition, there are limited reports on the study of fracture-mechanics

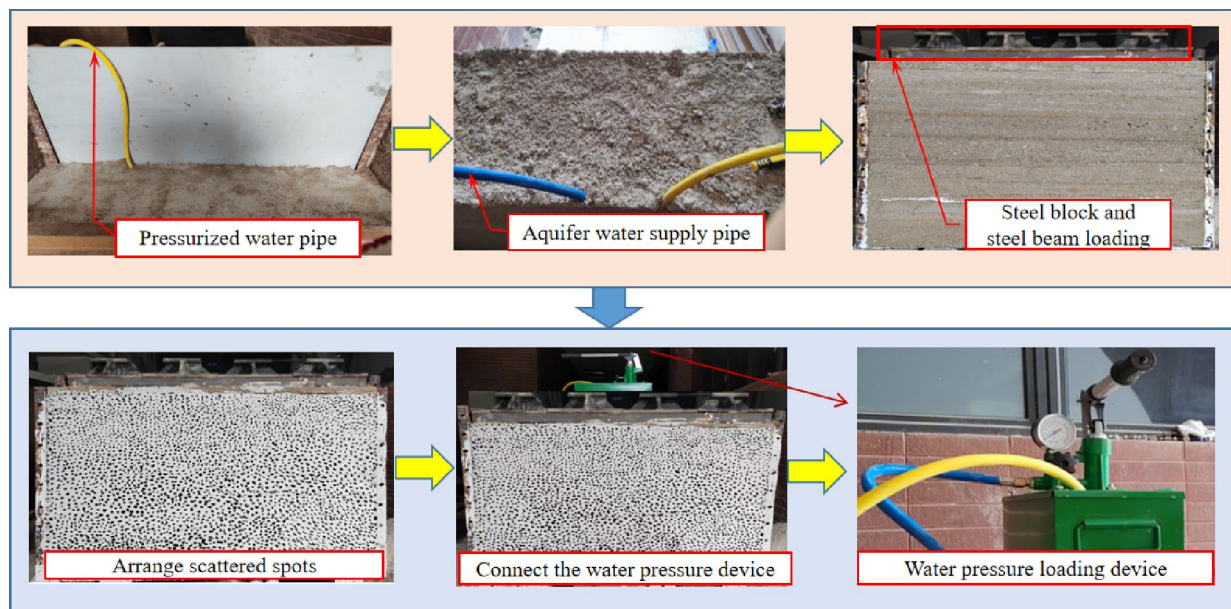
characteristics of aquicludes during karst water loss in thick aquifers under the influence of mining activities. Therefore, this paper will comprehensively consider the influences of mining, hydro-mechanical coupling, and water loss in thick aquifers, and deeply study the failure mechanism, movement characteristics, and fracture-mechanics characteristics of overlying strata under thick aquifers. The research results can provide a theoretical basis for the prevention and control of mine-water inrush, roof disasters, and surface ecological damage.

## 2 Engineering Background

The main coal seam of the Daojiao coal mine in Guizhou province is C3, with an average thickness of 2.02 m, a buried depth of 200–350 m, and an average dip angle of 7°. The overlying strata contain multiple aquifers with a specific hydraulic connection, and the average buried depth of static water level is 10 m. Moreover, it can be inferred that the distance of the bottom of the first thick fissure aquifer from the static water level is about 180 m. Taking 138 workface of the Daojiao coal mine as an engineering background, fully mechanized longwall coal-mining method was adopted. In the process of coal mining, the shearer continuously carried out cutting coal along the workface, and then the scraper conveyor transported the cut coal out of the workface. In addition, hydraulic supports were used to maintain the stability of the roof. Moreover, the treatment method of the goaf was the full caving. Meanwhile, the water generated during mining was mainly discharged from the workface through the drainage system, including drainage roadway,

**Table 1** Similar simulation parameters

Rock type	Thickness of stratum (m)	Model thickness (cm)	Total weight of material (kg)	Ratio (river sand:lime:gypsum)	River sand (kg)	Lime (kg)	Gypsum (kg)
Mudstone	10	8.33	63.28	14:1:1	55.37	3.96	3.96
Limestone	50	41.67	284.77	15:2:1	237.30	31.64	15.82
Sandy mudstone	24	20.00	126.56	40:3:2	112.50	8.44	5.63
Mudstone	4	3.33	23.91	14:1:1	20.92	1.49	1.49
Sandy mudstone	4.5	3.75	23.73	40:3:2	21.09	1.58	1.05
Carbon mudstone	2.5	2.08	14.36	55:4:3	12.73	0.93	0.93
C3 coal seam	2	1.67	6.89	60:3:2	6.36	0.32	0.21
Tonstein	10	8.33	52.73	17:1:3	42.69	2.51	7.53
C1 coal seam	1	0.83	3.45	60:3:2	3.18	0.16	0.11
Mudstone	12	10.00	71.72	14:1:1	62.75	4.48	4.48

**Fig. 8** Experimental operation process

drainage equipment, and drainage pipeline. The primary-overlying strata can be divided into ten layers from top to bottom. Figure 1 illustrates the lithology and thickness of each layer.

### 3 Analysis of Failure Mechanism of Overlying Strata with a Thick Aquifer

Figure 2 illustrates the failure mechanism and movement laws of overburden under thick aquifer conditions. Under the influence of mining activities, the deformation and destruction of overburden rock extended gradually from the bottom to the top. The movement of different rock layers was not

synchronous, coupled with the differences in the lithology of different rock layers, which resulted in the separation of the rock layers. Thus, it provided a large separation space for groundwater, especially between the aquifer and the aquiclude. On the other hand, the hydrostatic pressure and head difference in the aquifer promoted the increase of the separation space between the aquifer and the aquiclude, and a large amount of water in the aquifer can accumulate in the space while maintaining uniform stresses on the entire lower bedrock. In addition, the exposed length of the aquiclude and the hydrostatic pressure of overlying rock layers increased with the continuous advancing of the workface. Moreover, the stretching and bending damage in the overlying strata occurred when the load exceeded the self-generated strength,

leading to the upward development of cracks connecting the space of water accumulation with the water-bearing layer.

Due to the large thickness and high strength of the aquiclude, the mechanical analysis model of the fixed beam at both ends can be established when the aquiclude was used as the primary rock layer for calculation (Kang and Wang 2002), as shown in Fig. 3.

According to the mechanical model before and after the initial breaking of the overlying strata, the stress of the fixed beam was obtained by employing elastic mechanics as follows (Shi and Han 1987).

$$\begin{cases} \sigma_x = \frac{4q}{h^3}y^3 + \left(\frac{2ql^2}{h^3} - \frac{3q}{5h}\right)y - \frac{6q}{h^3}x^2y \\ \sigma_y = \frac{3q}{2h}y - \frac{2q}{h^3}y^3 - \frac{q}{2} \\ \tau_{xy} = \frac{6q}{h^3}xy^2 - \frac{3q}{2h}x \end{cases} \quad (1)$$

When the hydrostatic head above the aquifuge is  $h_0$ , the hydrostatic pressure  $P$  on the aquifuge can be expressed as follows.

$$P = \rho gh_0 \quad (2)$$

where  $\rho$  is the density of water,  $1000 \text{ kg/m}^3$ ;  $g$  is the acceleration of gravity,  $9.81 \text{ m/s}^2$ ;  $h_0$  is the height of water head,  $m$ .

When the buried depth of the aquiclude is  $H$ , the load  $q$  of the aquiclude is the sum of the hydrostatic pressure and the pressure of the overlying strata as follows.

$$q = P + \gamma H \quad (3)$$

where  $\gamma$  is the bulk density of the rock,  $\text{kN/m}^3$ .

Combining Eqs. (1), (2), and (3), the stress components of the aquiclude beam structure are expressed as follows.

$$\begin{cases} \sigma_x = (\rho gh_0 + \gamma H) \left( \frac{4}{h^3}y^3 + \frac{2l^2y}{h^3} - \frac{3y}{5h} - \frac{6x^2y}{h^3} \right) \\ \sigma_y = \left( \frac{3}{2h}y - \frac{2}{h^3}y^3 - \frac{1}{2} \right) (\rho gh_0 + \gamma H) \\ \tau_{xy} = \left( \frac{6}{h^3}xy^2 - \frac{3}{2h}x \right) (\rho gh_0 + \gamma H) \end{cases} \quad (4)$$

According to the actual geologic conditions of Daojiao coal mine, the thickness of aquiclude  $h$  is 24 m, the buried depth of aquiclude  $H$  is 190 m, and the height of the static water head is 180 m. To facilitate the analysis of the stress-distribution characteristics of the rock-beam structure of the aquiclude,  $l$  is determined as 50 m. According to the stress-component expression, the  $\sigma_{xx}$  and  $\sigma_{xy}$  stress-component



Fig. 9 Digital speckle monitoring acquisition system

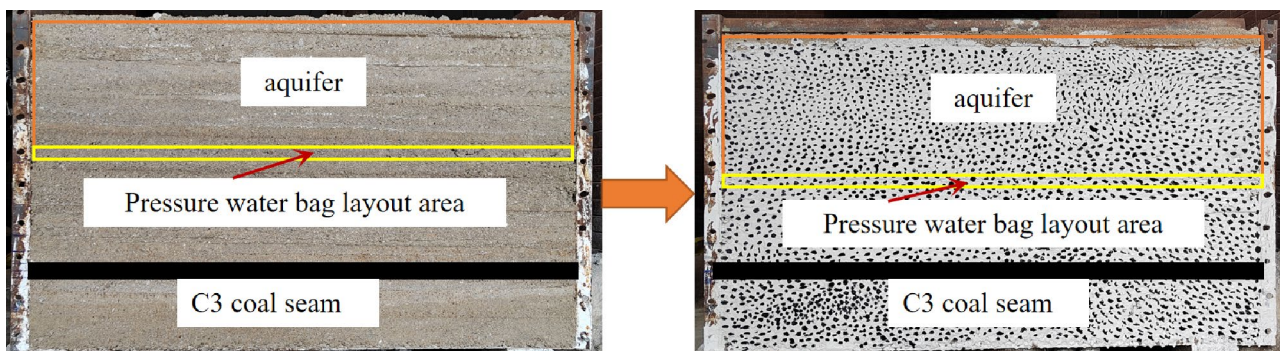
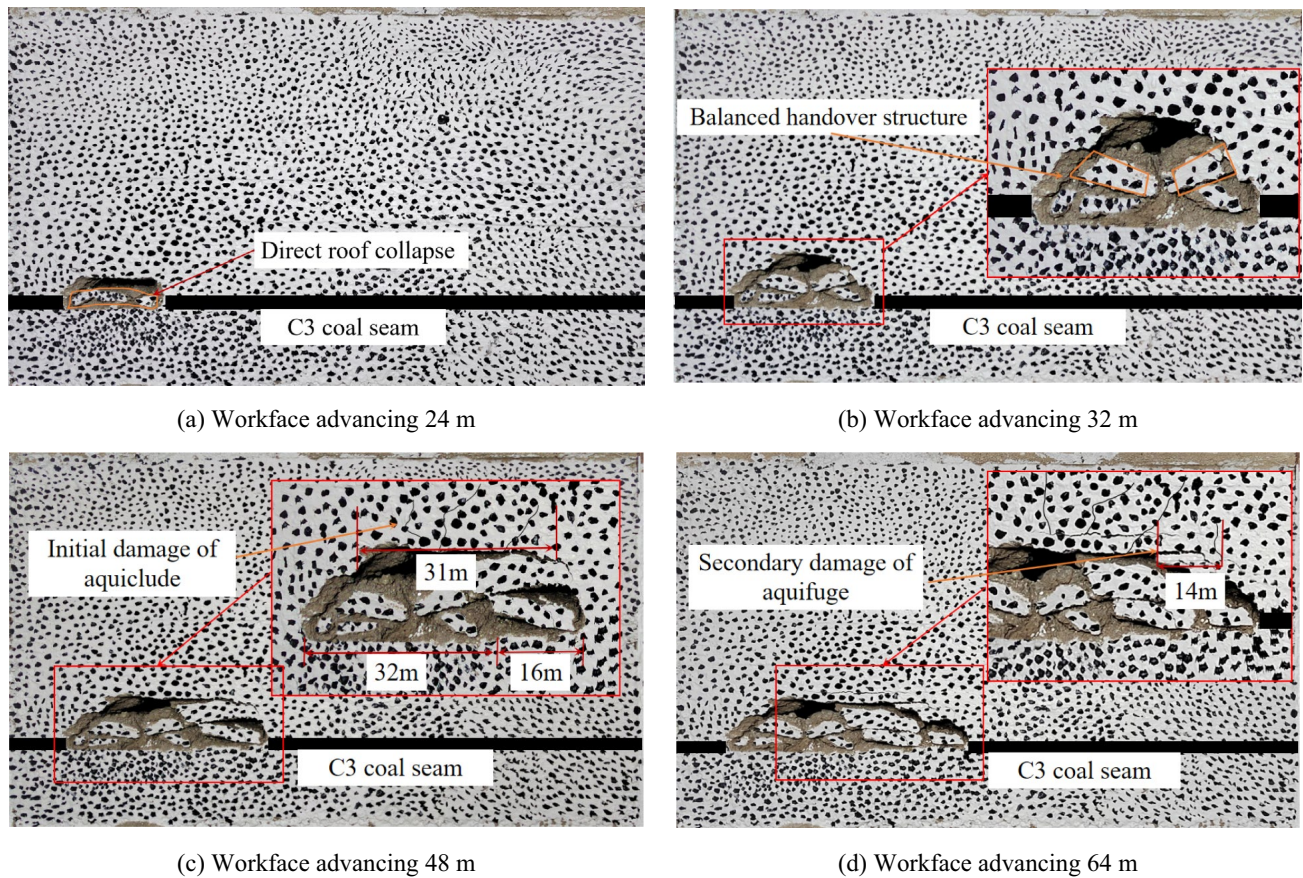


Fig. 10 Model before excavation





**Fig. 11** Distribution characteristics of overlying strata until advancing 64 m. **a** Workface advancing 24 m. **b** Workface advancing 32 m. **c** Workface advancing 48 m. **d** Workface advancing 64 m

programs of the aquiclude rock-beam structure are drawn by MATLAB, as shown in Fig. 4.

By analyzing the stress function and Fig. 4, it can be seen that the shear stress at the  $x = 0$  section in the middle of the rock beam is zero, and the tensile stress reaches the maximum at the point of  $(0, 0.5h)$ . The maximum tensile stress can be obtained as follows.

$$\sigma_{t \max} = (\rho gh_0 + \gamma H) \left( \frac{1}{5} + \frac{l^2}{h^2} \right) \quad (5)$$

According to the first strength theory, the expression of the initial breaking distance of the aquifuge under the ultimate tensile strength can be obtained as follows.

$$L_s = 2h \sqrt{\frac{[\sigma]}{(\rho gh_0 + \gamma H)n} - \frac{1}{5}} \quad (6)$$

where  $[\sigma]$  is the tensile strength of aquiclude, MPa;  $n$  is the safety factor.

As shown in Fig. 5, the mechanical analysis model of the cantilever beam was established, and the stress-component

expression of periodic breaking of aquiclude can be obtained as follows (Kang and Wang 2002).

$$\begin{cases} \sigma_x = (\rho gh_0 + \gamma H) \left( \frac{12l}{h^3}xy + \frac{4}{h^3}y^3 - \frac{3}{5h}y - \frac{6}{h^3}yl^2 - \frac{6}{h^3}x^2y \right) \\ \sigma_y = \left( \frac{3}{2h}y - \frac{2}{h^3}y^3 - \frac{1}{2} \right) (\rho gh_0 + \gamma H) \\ \tau_{xy} = \left( \frac{6}{h^3}xy^2 - \frac{3}{2h}x - \frac{6l}{h^3}y^2 + \frac{3l}{2h} \right) (\rho gh_0 + \gamma H) \end{cases} \quad (7)$$

According to the expression of stress component, the cloud diagram of three stress components is drawn as shown in Fig. 6.

By analyzing the stress function and Fig. 6, it can be seen that the maximum tensile stress can be observed in the middle of the rock beam  $(0, -0.5h)$ , and the maximum principal stress is obtained as follows.

$$\sigma_{t \max} = \left( \frac{3l^2}{h^2} - \frac{1}{5} \right) (\rho gh_0 + \gamma H) \quad (8)$$



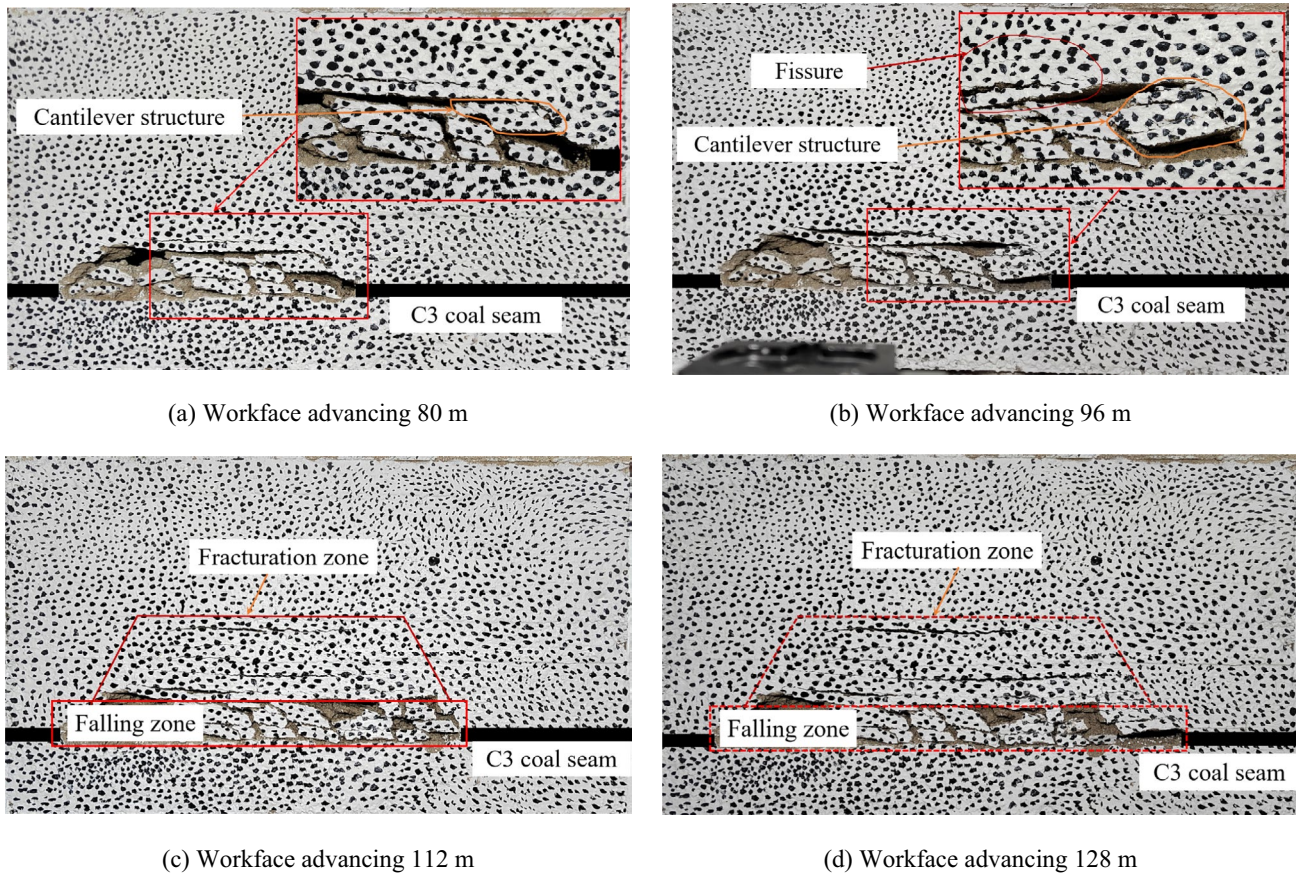


**Fig. 12** Deformation characteristics of overlying strata. **a** Workface advancing 80 m. **b** Workface advancing 96 m. **c** Workface advancing 112 m. **d** Workface advancing 128 m

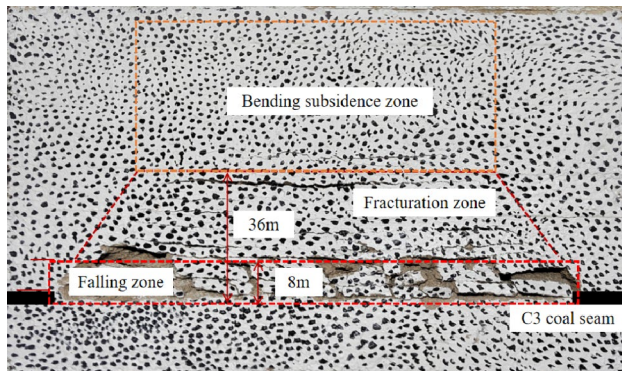


**Fig. 13** Deformation characteristics of overlying strata when workface advancing to 144 m

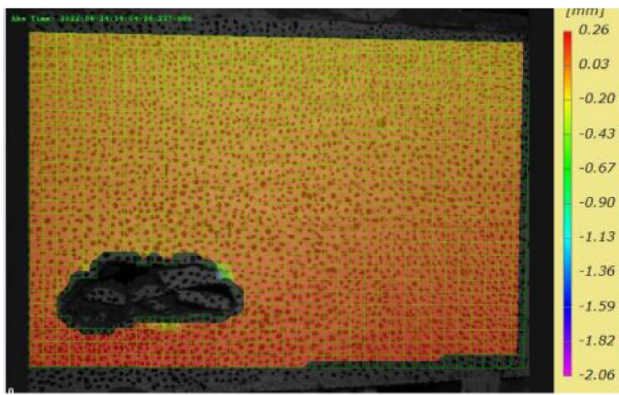
Similarly, according to the maximum tensile stress theory, the expression of the periodic breaking distance of the aquifuge can be obtained as follows.

$$L_p = h \sqrt{\frac{5[\sigma] + (\rho gh_0 + \gamma H)}{15n(\rho gh_0 + \gamma H)}} \tag{9}$$

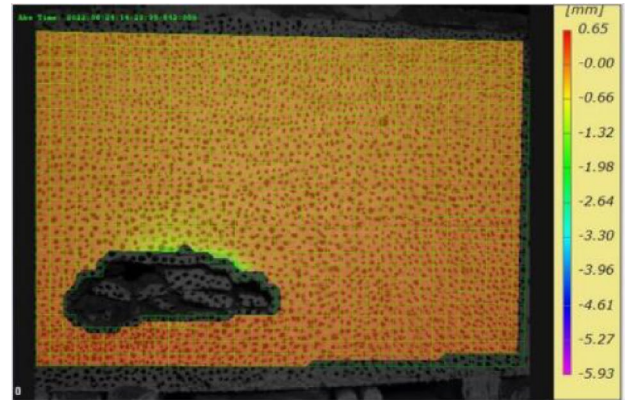
According to the actual geologic conditions of Daojiao coal mine, the tensile strength  $[\sigma]$  of aquiclude is 3.31 MPa, and the safety factor  $n$  is 1.2. Substituting the relevant parameters into Eqs. (6) and (9), the initial and periodic breaking distances of the aquifuge are 31.63 and 14.02 m, respectively.

Generally, the water head height of the aquifer is easily affected by the season, sometimes increasing or decreasing, which leads to a change of hydrostatic pressure. To illustrate the influence of the water head height of the aquifer on the breaking distance of the aquifuge, the water head  $h_0$  is selected as a variable. Combined with Eqs. (6) and (9), the variation law of the initial and periodic breaking distance of the aquifuge can be obtained as shown in Fig. 7. It can be seen that the initial and periodic breaking distances of the roof aquiclude linear increase with the increase of the tensile strength of the rock and linear decrease with the increase of the hydrostatic head height.

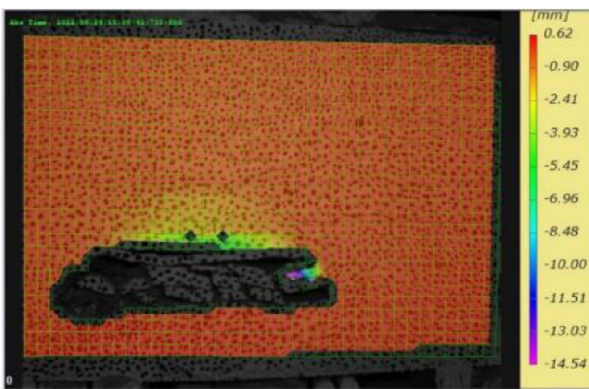




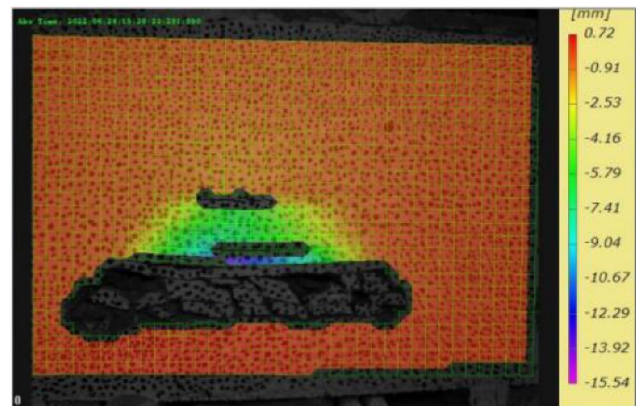
(a) Workface advancing 48 m



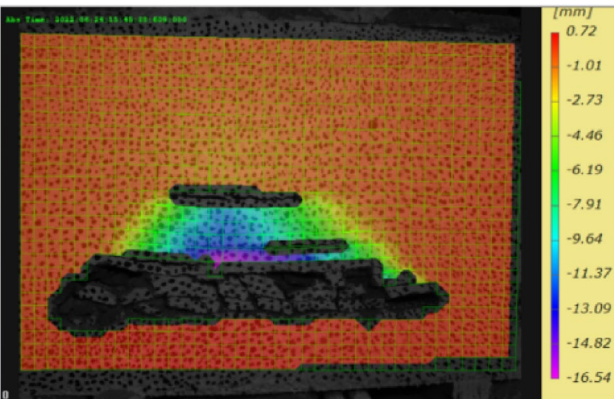
(b) Workface advancing 64 m



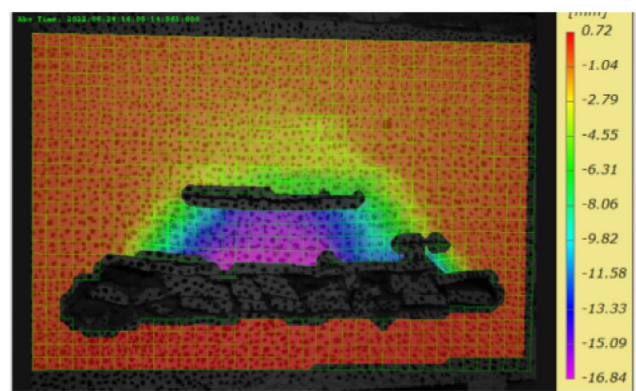
(c) Workface advancing 96m



(d) Workface advancing 112m



(e) Workface advancing 128m



(f) Workface advancing 144m

**Fig. 14** Displacement characteristics of overlying strata mining with multi-aquifer. **a** Workface advancing 48 m. **b** Workface advancing 64 m. **c** Workface advancing 96 m. **d** Workface advancing 112 m. **e** Workface advancing 128 m. **f** Workface advancing 144 m

## 4 Physical Simulation Considering Solid–Fluid Coupling

### 4.1 Material Selection

The size of the experimental test bench is 1.5 m × 0.3 m × 1.2 m in the direction of length, width, and height, respectively. Moreover, in this study, the similarity ratio of geometric ( $a_l$ ), gravity ( $a_g$ ), bulk density ( $a_\gamma$ ), and stress ( $a_\sigma$ ) is 120, 1, 1.6, and 192, respectively.

The deformation and movement characteristics of overlying strata depend on the strength of rock mass along with different failure forms. This study selected ordinary river sand as aggregate with a particle size of <1.6 mm, while lime and gypsum were selected as cementing materials. Mica powder was used as stratification material to distinguish different lithologic strata. In addition, foam was used to distinguish the coal and rock boundary, which facilitated the subsequent mining work and reduced the influence of human factors on the damage of overlying strata. The amount of similar materials in each model layer is calculated as follows.

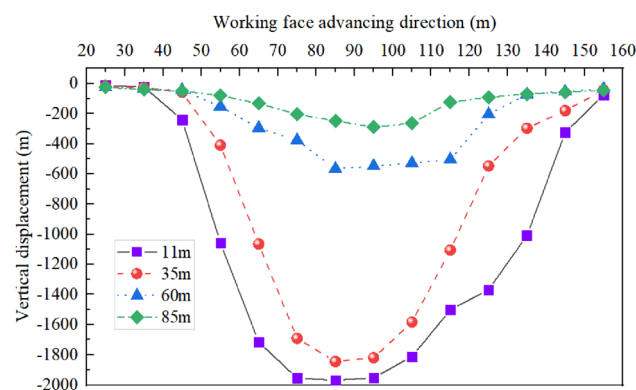
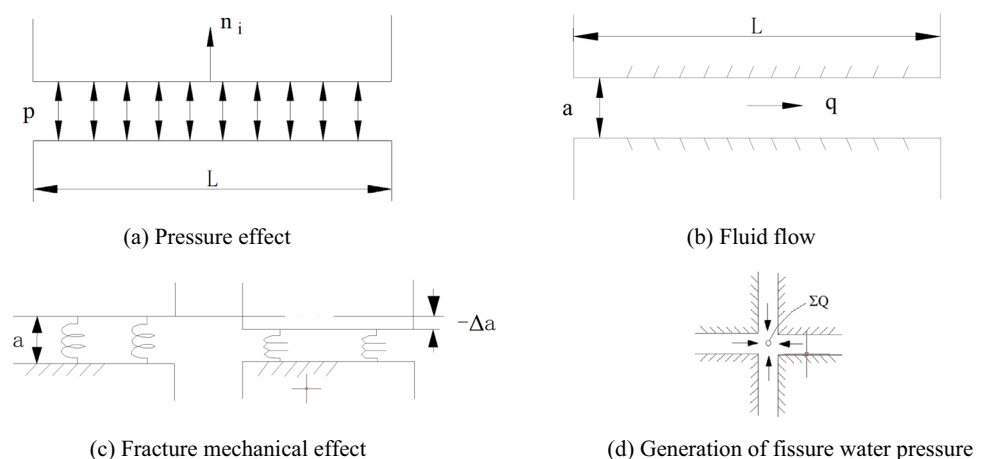


Fig. 15 Vertical displacement curves of monitoring lines

Fig. 16 Solid–liquid interaction. **a** Pressure effect. **b** Fluid flow. **c** Fracture mechanical effect. **d** Generation of fissure water pressure



$$G = Lbh\gamma_m \tag{10}$$

where  $G$  is the weight of each layer material, kg;  $L$  is the length of the model,  $m$ ;  $B$  is the thickness of the model;  $h$  is the height of each layer;  $\gamma_m$  is the bulk density of each layer.

The material ratio is determined according to the tensile strength of overlying strata and the compressive strength of coal seam and floor strata. Table 1 illustrates the thickness and material ratio of each layer.

### 4.2 Experimental Process

Quantitative river sand, lime, gypsum, and water were uniformly mixed to construct each rock layer in the model from bottom to top. To simulate the water pressure in the thick aquifer approximately, it was necessary to make a unique treatment for the laying of water-bearing strata. As shown in Fig. 8, a pressure water bag was arranged between the bottom of the aquifer and the upper part of the aquiclude, which was connected to the pressure pipe matched with the pressure test pump. In the subsequent mining process, the manual pressure test pump injected water into the bag until the water pressure reached the preset value. Moreover, in order to approximately simulate the water-bearing state of the aquifer and the solid–fluid coupling characteristics during the mining process, it was necessary to pre-bury the water-conducting pipe in the aquifer, and the appropriate water was slowly introduced until the aquifer was in a saturated state.

Fixed constraints were set up in the bottom, left, and right sides of the model, while the upper boundary was loaded with equivalent rock weight using steel beam blocks. According to the geologic conditions of the coal mine, the average buried depth of the C3 coal seam was 225 m, and the distance between the upper parts of the rock layer and the ground in the simulation range was 130 m. Therefore, the

required loading for the upper boundary of the model can be calculated as follows.

$$P = \frac{gh\gamma_p}{a_x a_y} = \frac{9.81 \times 130 \times 2.5}{120 \times 1.6} = 16.6 \text{ kN/m}^2 = 0.0166 \text{ MPa} \quad (11)$$

where  $g$  is the acceleration of gravity,  $9.81 \text{ m/s}^2$ ;  $h$  is the distance from the upper part of the rock layer to the ground in the simulation range,  $130 \text{ m}$ ;  $\gamma_p$  is rock bulk density, taking the average value of  $2.5 \text{ t/m}^3$ .

Two thick aquifers can be observed in the mining area, and there was a poor water resistance aquiclude layer (mudstone) with a thickness of  $8\text{--}15 \text{ m}$  between the two aquifers. Under the natural conditions, the average static water level of the mining area was  $10 \text{ m}$ , and two aquifers had a certain hydraulic connection. It can be inferred that the rock stratum from the bottom of the first aquifer to the ground was immersed. Therefore, the bottom of the first aquifer in the prototype produced  $1.8 \text{ MPa}$  head pressure along the direction of gravity acting on the lower rock strata. According to the above similarity ratio of stress, the pressure water bag should reach  $0.0094 \text{ MPa}$ .

The mining height of the coal seam in the model was  $1.67 \text{ cm}$ , which corresponded to the thickness of the coal seam as  $2 \text{ m}$  in practical conditions (according to the geometric similarity ratio  $120$ ), and  $15 \text{ cm}$  coal pillars on both sides were retained to eliminate the influence of the

boundary in the model. Meanwhile, the mining direction was from left to right with each excavation step of  $6.7 \text{ cm}$  (corresponding to  $8 \text{ m}$  in practical conditions), and the total advance distance of the workface was  $120 \text{ cm}$  (corresponding to  $144 \text{ m}$  in practical conditions). In the following analysis of the experimental results, the actual advancing distance of the workface in practical conditions was adopted.

As shown in Fig. 9, the three-dimensional displacement and strain visualization digital speckle monitoring technology system was used to monitor and record the displacement of overlying strata and the dynamic evolution characteristics of overlying strata under different advancing distances. To meet the observation and recording of the monitoring equipment, the lime slurry was used to paint the surface of the model. After drying, the surface was randomly spotted with ink to form random speckles as shown in Fig. 10.

## 4.3 Experimental Results

### 4.3.1 Analysis of Failure Characteristics and Movement Laws of Overlying Strata

As shown in Fig. 11, it can be illustrated that two sides of the immediate roof were cut along the coal wall when the coal mining face advanced to  $24 \text{ m}$ . The immediate roof collapsed with the continuous advance of the workface. Meanwhile, the initial weighting of the main roof can be observed

**Table 2** Mechanical and hydraulic parameters of coal and rock mass

Rock type	Density ( $\text{kg/m}^3$ )	Bulk modulus / (GPa)	Shear modulus / (GPa)	Friction angle / ( $^\circ$ )	Cohesion / (MPa)	Tensile strength / (MPa)	Compressive strength / (MPa)
Limestone	2430	11.1	8.3	35	2.4	4.4	43.52
Sandy mudstone	2250	10.2	6.1	30	1.8	3.6	31.6
Mudstone	2550	5.8	3.2	30	1.2	3.25	36.3
Carbon mudstone	2450	4.3	2.8	30	0.7	1.8	17.8
Coal seam	1470	1.19	0.82	25	1.3	1.79	18.4
Tonstein	2250	4.39	2.27	27	4.9	3.8	40.3
Water	1000	–	–	–	–	–	–

**Table 3** Mechanical parameters of rock joint

Rock type	Normal stiffness / (GPa)	Tangential stiffness / (GPa)	Internal friction angle / ( $^\circ$ )	Cohesion / (MPa)	Tensile strength / (MPa)	Permeability coefficient / ( $\text{pa}^{-1} \text{ s}^{-1}$ )	Initial gap width / (mm)	Residual gap width / (mm)
Limestone	13.1	9.3	35	1.4	0.4	110	0.2	0.05
Sandy mudstone	12.2	7.4	28	0.9	0.2	83	0.01	0.005
Mudstone	7.8	6.2	29	0.5	0.35	83	0.01	0.005
Carbon mudstone	5.3	4.8	28	0.7	0.82	83	0.01	0.005
Coal seam	2.19	1.72	26	1.3	0.79	83	0.01	0.005
Tonstein	6.29	4.27	17	4.1	1.8	83	0.01	0.005



at the advancing distance of 32 m. Under the support of the collapsed rock, a triangular arch equilibrium structure can be formed, and the breaking point was located in the middle of the goaf. When the advancing distance of the workface to 48 m, The main roof is broken again, that is, the periodic weighting of the main roof. In addition, the exposed length of the aquifuge above the main roof is 31 m, and the initial breaking occurs, that is, the initial breaking distance of the aquifuge is 31 m. With the continuous advancement of the workface, the range of mining-induced failure areas increased, and the periodic pressure was more obvious. The previous cantilever beam completely collapsed, accompanying with a few cracks extend to the above roof when the working face advanced to 64 m. Moreover, the exposed length of the aquifuge is 14 m, and it is broken again, that is, the periodic breaking distance of the aquifuge is 14 m.

As shown in Fig. 12, the cantilever-beam structure can be observed again on the side of the coal wall, along with a small number of cracks gradually expanding to the aquiclude when the workface advancing to 96 m. However, the crack-propagation speed of overlying strata changed abruptly, accompanying with the significant subsidence of overlying strata and resulting in a large separation space at the bottom of the aquifer when the workface advanced to 112 m. It can be explained that the aquiclude was regarded as the water-resisting key stratum with hard rock, and it had a strong bearing capacity to protect the overlying strata before reaching its limit span. With the continuous advancement of the workface, the hanging distance of the roof became prominent, and the load acting on the aquiclude gradually increased. After exceeding its bearing capacity, tensile failure can be occurred. In addition, due to the low strength of the upper rock stratum, it can bend and sink to cause a sudden change in the crack-propagation speed of the overlying strata and the subsidence speed of the roof. On the other hand, the water can penetrate the aquiclude through the mining fissure channels to reduce its strength and aggravate its deformation and failure speed.

In the process of advancing distance from 96 to 112 m in the workface, the internal cracks of the rock layer were

penetrated with the aquiclude, which destroyed its integrity and makes it lose the water isolation effect. The strength of the aquiclude was greatly weakened after water infiltration. In addition, the roof hanging area increased with the advancement of the workface, and the tensile failure can be occurred in the roof under the weight of the applied load by the overlying strata exceeding the bearing capacity of the roof.

As shown in Fig. 13, the immediate roof collapsed continuously, and the main roof can form a cantilever beam continuously after the working face advancing to 144 m. The cantilever beam was broken and collapsed along the coal wall after reaching a certain length. In the whole process, The initial and periodic breaking distances of the aquiclude were 31 and 14 m, respectively, which were similar to the theoretical calculation results. In addition, the height of the caving zone remained almost constant at about 8 m, and the height of water-conducting fractured zone was stable at about 36 m to form the three-zone distribution areas.

When the mining height and burial depth of coal seam were <3 and 300 m, respectively, the height of caving zone and the height of water-conducting fractured zone can be calculated according to the empirical formulas (China National Bureau of Coal Industry, 2000).

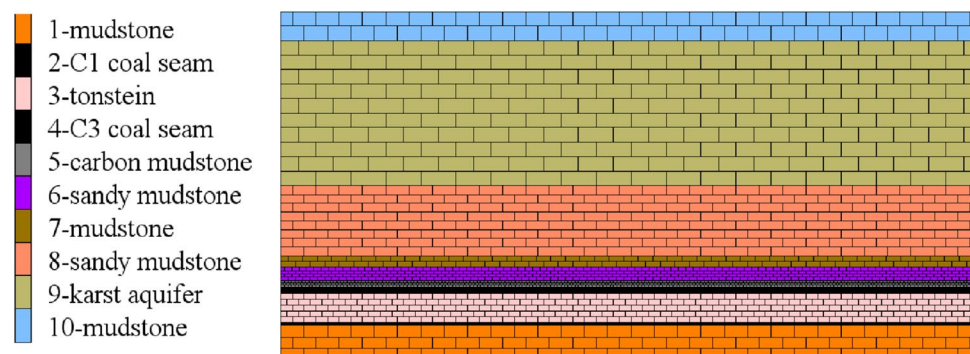
$$H_c = \frac{100 \sum M}{4.7 \sum M + 19} \pm 2.2 \quad (12)$$

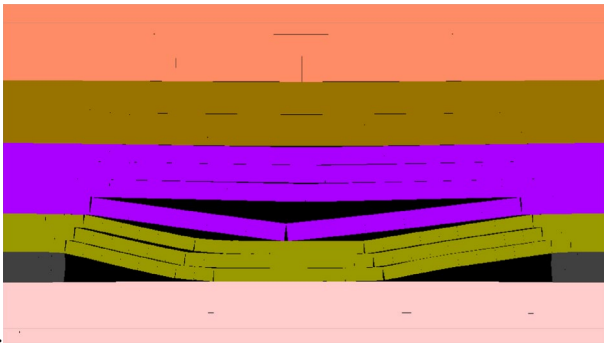
$$H_f = \frac{100 \sum M}{1.6 \sum M + 3.6} \pm 5.6 \quad (13)$$

where  $H_c$  is the HCZ, m;  $H_f$  is the HWCFZ, m;  $M$  is the mining thickness of the coal seam, taking 2.02 m for  $M$ .

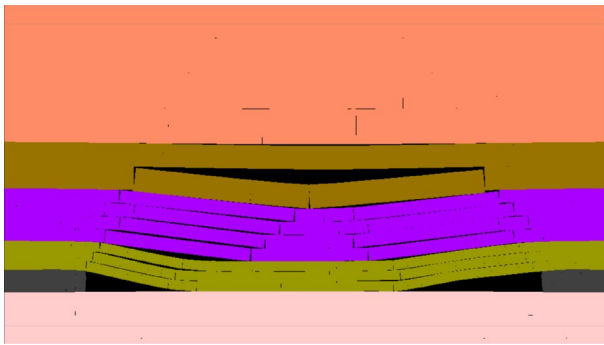
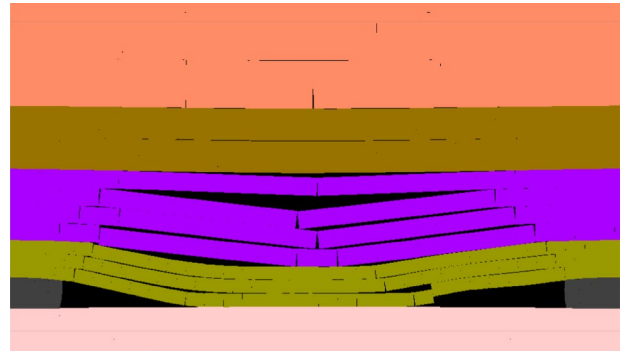
According to the above empirical formula, the height of caving zone in the 138 working face is 4.8–9.2 m, and the height of water-conducting fractured zone is 23.8–35.0 m. Compared with the results of the physical experiment, the height of caving zone is basically the same, while the height of water-conducting fractured zone is slightly lower. Therefore, from the perspective of safety, the results of physical

Fig. 17 Numerical model

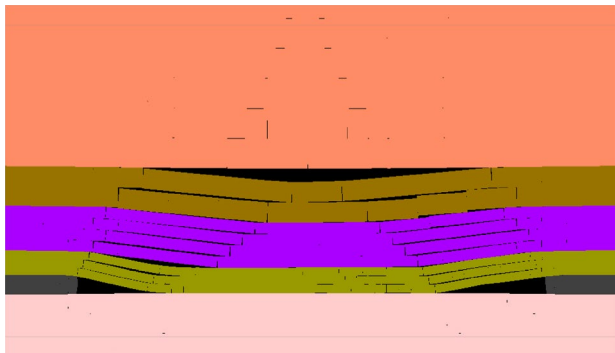
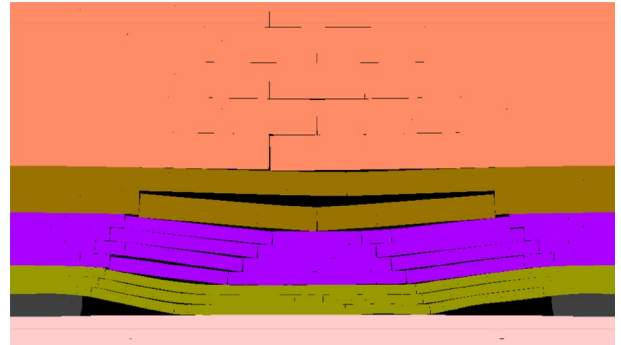




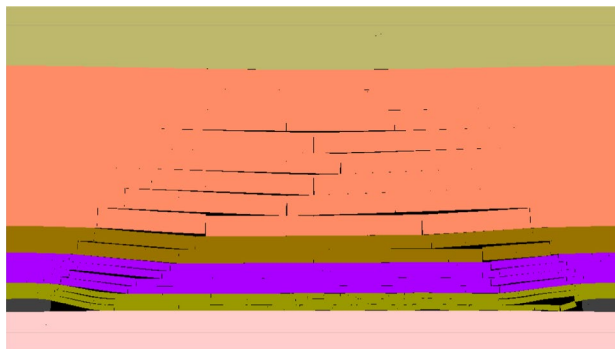
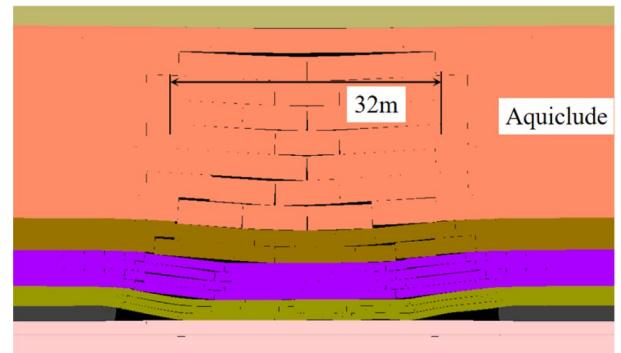
(a) Workface advancing 32m



(b) Workface advancing 40m



(c) Workface advancing 48m



(d) Workface advancing 80m

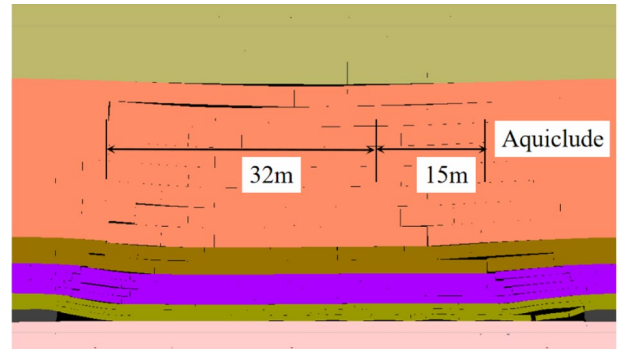


**Fig. 18** Movement characteristics of overlying strata (*left* was CI, *right* was CII). **a** Workface advancing 32 m. **b** Workface advancing 40 m. **c** Workface advancing 48 m. **d** Workface advancing 80 m

experiments are conducive to the prevention and control of water inrush in coal seam mining.

#### 4.3.2 Displacement Distribution Characteristics of Overlying Strata Based on Digital Speckle Technology

Before the excavation process, four displacement monitoring lines were arranged at 11, 35, 60, and 85 m from the coal seam, and 14 recording points were set up for each monitoring line to record the vertical displacement of overlying strata at different advance distances of the workface.

Figure 14 illustrates the vertical displacement cloud images of the whole model through a three-dimensional displacement and strain visualization digital speckle monitoring system. It can be found that the deformation and failure of the roof near the excavation area were severe, and the collapse of the surface in the model and the prominent separation characteristics of each layer can be observed. Thus, the speckles were destructed, and the digital speckle algorithm in the area with severe deformation cannot be identified. This area can be approximately regarded as a caving zone. With the continuous advancement of the workface, the displacement of overlying strata was more obviously affected by the mining activities, and the largest subsidence of overlying strata was near the excavation area. Moreover, the vertical displacement gradient of overlying strata gradually decreased from bottom to top. In addition, the height of the unidentified area near the excavation area gradually increased, indicating that the collapsed height and failure degree of overlying strata increased with the advancement of the workface. When the workface advancing to 112 m, the vertical displacement of overlying strata increased sharply, and the displacement gradient increased from bottom to top, corresponding to the sudden changing in the crack-propagation speed and the subsidence speed of overlying strata, as mentioned before. Meanwhile, the maximum vertical displacement point of the overlying strata moved from the middle of the goaf to the left near, indicating that the overlying strata were still in a state of slow subsidence affected by mining. On the other hand, the water-conducting fracture had expanded to the bottom of the aquifer, and water gradually diffused into the goaf, resulting in the soaked and weakened rock in the goaf. Therefore, the strength of the collapsed roof in the goaf reduced, and it can be easily compacted.

The overlying strata in the goaf sank with funnel type and the vertical displacement curves of different strata layers generally distributed symmetrically as shown in Fig. 15. Moreover, the vertical displacement of overlying strata in

the goaf decreased with the increase of the distance from the coal seam, while the vertical displacement of overlying strata near the open-off cut and the coal wall increased with the increase of the distance from the coal seam although the increment value was not apparent. The maximum vertical displacement of overlying strata away from coal seams 11, 35, 60, and 85 m was 1990, 1850, 580, and 300 mm, respectively.

## 5 Numerical Simulation with Solid–Fluid Coupling

### 5.1 Fluid–Solid Coupling Principle

UDEC assumes that the block is impermeable and the fluid flow only occurs in the fracture. In the solid–liquid coupling analysis, the mechanical deformation of the block fracture affects the fracture penetration rate and the fracture pore-water pressure, and vice versa. Figure 16 shows the basic principle of solid–liquid mechanical coupling in the UDEC-simulation process. The expression for calculating the force of fluid acting on the rock block is obtained as follows.

$$F_i = pn_iL \quad (14)$$

where  $F_i$  is the force of the fluid acting on the rock,  $p$  is the fluid pressure, and  $L$  is the length between the two domains.

Moreover, the fluid flow rate can be determined as follows.

$$q = -k_j a^3 \frac{\Delta p}{L} \quad (15)$$

where  $q$  is the flow rate;  $k_j$  is the fracture permeability coefficient (the theoretical value is  $1/12 \mu$ );  $\mu$  is the dynamic viscosity coefficient of the fluid;  $a$  is hydraulic gap width;  $\Delta p$  is the fluid pressure difference.

The change in fissure width can be expressed as follows.

$$a = a_0 + \Delta a \quad (16)$$

where  $a$  is the crack width,  $a_0$  is the initial crack width,  $\Delta a$  is the change of crack width.

Therefore, the generation of water pressure at the fracture intersection can be calculated as follows.

$$\Delta p = \frac{K_w}{V} \left( \sum Q \Delta t - \Delta V \right) \quad (17)$$

where  $K_w$  is the bulk modulus of fluid;  $V$  is the average value before and after the change of fracture volume;  $\sum Q$  is the total flow of nodes;  $\Delta t$  is the time step difference of change;  $\Delta V$  is the change of fracture volume.

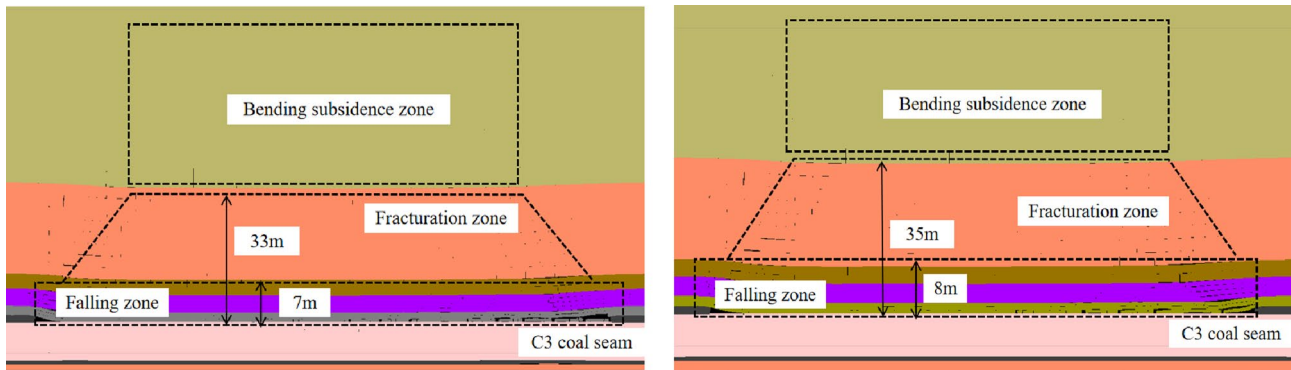


Fig. 19 Three-zone distribution of overlying strata at the end of mining (left was CI, right was CII)

## 5.2 Numerical Model Without Water Pressure in Thick Aquifers (CI)

Taking the 138 workface of the Daojiao coal mine as an engineering background, the numerical model was established with the length and height of 240 and 120 m, respectively. The average buried depth of the coal seam was about 225 m, and the upper boundary was loaded with an equivalent rock mass weight of 3.2 MPa. According to the burial depth of the model and the pressure coefficient of 1.2, the vertical and horizontal initial stresses at the lower end of the model were 6.2 and 7.44 MPa, respectively. The stresses gradually decreased from bottom to top, and the vertical and horizontal stress gradients were  $-0.025$  and  $-0.03$  MPa/m, respectively. The boundary on both sides was a fixed constraint in horizontal directions, and the bottom of the model was a fixed constraint in vertical directions. In the excavation process, 40 m coal pillars were set up on the left and right sides of the model to eliminate the boundary effect, and a total of 160 m in the strike direction were excavated. In addition, the yield failure criterion of the model adopted the Mohr–Coulomb criterion, and the Contact-Coulomb slip model was selected to solve the structural plane. Tables 2 and 3 given the mechanical and joint parameters of each rock layer in the numerical model.

## 5.3 Numerical Simulation with Water Pressure in Thick Aquifers (CII)

Based on the numerical model without water, a solid–fluid coupling model was adopted to simulate the multi-aquifer with water. According to the hydrogeological data in Daojiao coal mine, the water level of the mining area was buried at 10 m below the surface, and the two aquifers had a certain hydroallic connection. Thus, besides keeping the boundary conditions of the numerical model for aquifers with water consistent with the aquifers without water, a 1.8 MPa head pressure gradient along the vertical direction was applied at

the bottom of the first fissure aquifer in the model as the initial condition. The left- and right-lower boundaries were set at the impermeable boundaries, and the seepage calculation was carried out by setting flow steady. Other parameters and conditions were the same as the numerical model without water, and the numerical model is shown in Fig. 17.

## 5.4 Results of Numerical Simulation

### 5.4.1 Overlying Strata Failure Characteristics

The movement and failure characteristics of overlying strata are illustrated in Fig. 18, in which the left side is the results of CI condition and the right side is the results of CII condition. With the advance of the workface, the damage range of the overlying strata increased continuously, and a narrow triangular type can be formed in the area of the coal wall and open-off cut. Meanwhile, the overlying strata at the open-off cut in the goaf and the workface can form a cantilever-beam structure under the support of the coal wall.

When the workface of CI condition advancing to 32 m, the main roof was broken locally, and the fracture position was located in the middle of the goaf. With the workface advancing to 40 m, the main roof was broken along the middle of the goaf, and the pressure on the roof increased dramatically due to the occurrence of the first weighting stage. The whole failure process can be approximately regarded as tension-bending fractures. However, for the overlying strata containing water pressure in thick aquifers (CII), the main roof can be broken and the first weighting pressure was occurred when the workface advancing to 32 m (less 8 m than CI), and the fracture position was also located in the middle of the goaf. When the workface advancing to 48 m, it is observed that the aquifuge is first broken under the action of pore-water pressure, and the initial breaking distance is 32 m, accompanied by the formation of several separated spatial and transverse cracks. In comparison, the aquiclude in CI condition was still intact until the workface



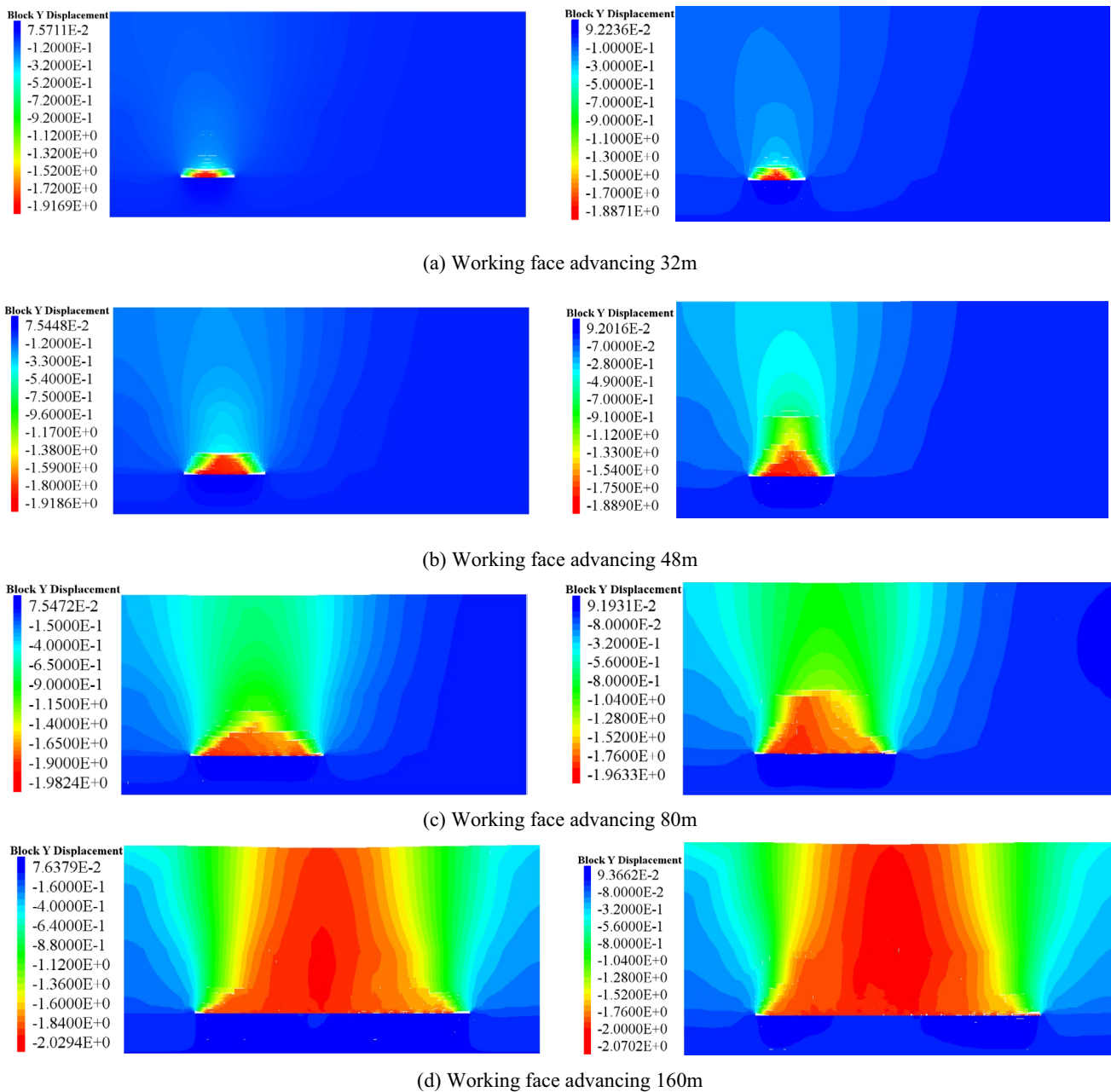


**Fig. 20** Vertical displacement distribution (left was CI, right was CII). **a** Working face advancing 32 m. **b** Working face advancing 48 m. **c** Working face advancing 80 m. **d** Working face advancing 160 m

advances to 80 m. In addition, the caving angle of overlying strata in CII condition was obviously larger than that of CI condition. When the workface advancing to 80 m in CII condition, the separation spaces and transverse cracks of the aquiclude above the middle of the goaf were obviously compacted, while the aquifuge above the working face was broken again along with the breaking distance of 15 m, and the aquifer shown overall bending subsidence. For both CI and CII conditions, the shape of overlying strata after collapse and accumulation in the middle of the goaf experienced a

process from a pyramid to a positive trapezoid. However, the evolution process of overlying strata in CII condition was faster than CI condition, and the bottom angle of the positive trapezoid in CII condition was also larger than CI condition.

Figure 19 illustrated the distribution characteristics of the three zones of the overlying strata in CI and CII conditions at the end of workface mining. It shown that the height of the caving zone and fracture zone in CII condition were 8 and 35 m, respectively, which were higher than that of CI condition. It was close to the results of

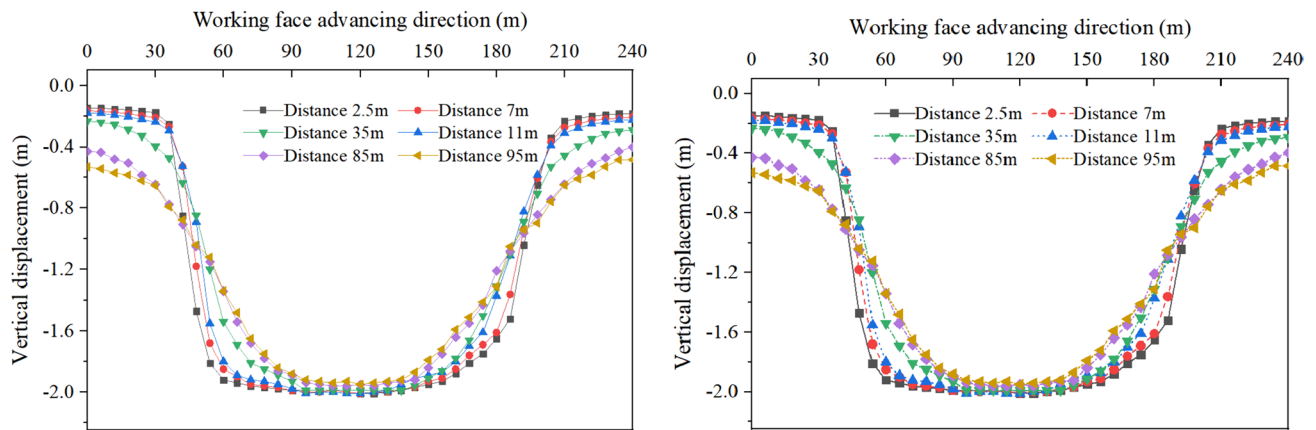


**Fig. 21** Vertical displacement curves of different layers when the working face advancing to 160 m

large-scale physical simulation test, indicating that the influence of water pressure on the distribution of the three zones of overlying strata was greatly obvious.

Through comparative analysis, water seepage and water pressure have a considerable influence on the movement and failure characteristics of overlying strata, especially for the first weighting distance of the roof, the broken distance of aquiclude, the caving angle of overlying strata, and the subsidence of both sides of goaf. Under the influence of mining activities, the internal cracks of the rock stratum penetrated through the aquiclude, providing the mining fissure channels for the water diffusing into the rock mass, and resulting in the decrease of the internal friction angle and cohesion of rock mass. Coupled with the influence of water pressure, it can aggravate the degree of deformation and failure of overlying strata. Therefore, it can be further determined that the combined effect of water infiltration and water pressure were the main reasons for the sudden change of overburden fracture propagation speed and roof subsidence speed, which was consistent with the results of the large-scale physical simulation test.

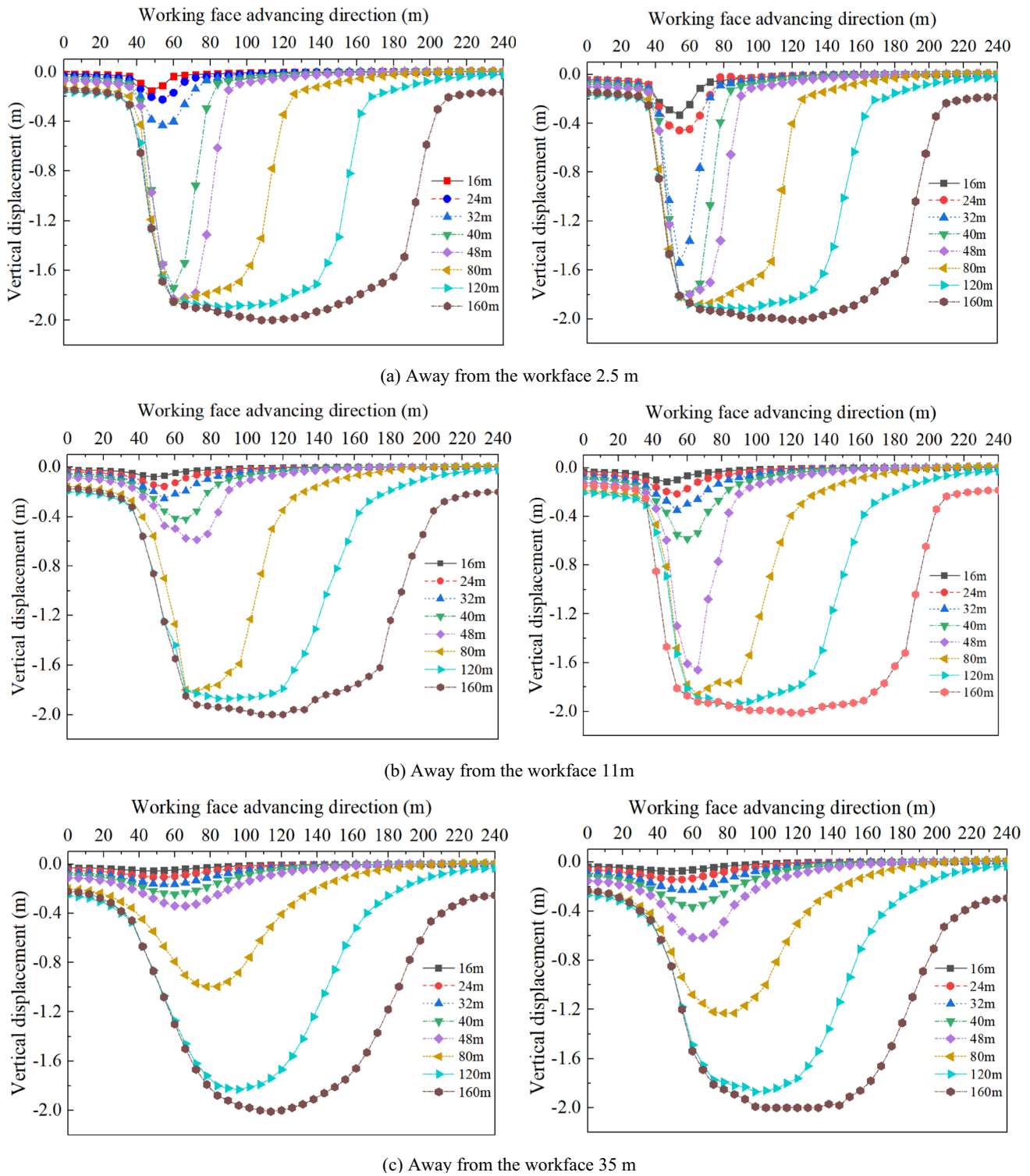
#### 5.4.2 Subsidence of Overlying Strata

Figure 20 illustrates the displacement distribution characteristics of overlying strata in CI and CII conditions (the left side was CI and the right was CII). It shown that the vertical displacement of the overlying strata increased with the advance of the workface, while the vertical displacement of the floor strata increased first and then decreased. In addition, the displacement of overlying strata above the aquiclude was limited in CI condition because the aquiclude was still intact until the workface advancing to 48 m with producing large deformation and damage of overlying strata. However, the rock strata below the aquiclude sank

considerably in CII condition. Meanwhile, the displacement difference between the upper and lower strata bounded by the aquiclude in CII condition is larger than that of CI condition at the workface advancing to 80 m. It can be explained that there was immense pore-water pressure between the aquiclude and the aquifer, which had a negative effect on the overlying strata below the aquiclude to accelerate its sinking speed and amount. On the other hand, the water pressure has a positive effect on the overlying strata above the aquiclude to hinder its settlement. With the advancement of the workface, the water-conducting fissure can be expanded to the overlying strata, causing continuous water loss and resulting in the decline of the water level and the decrease of water pressure.

Figure 21 illustrated the vertical displacement curves of different rock layers at various advancing distances of the working face in CI and CII conditions (the left side was CI, and the right was CII). It shown that the vertical displacement of the overlying strata in different rock layers above the goaf increased with the continuous advance of the workface, and the vertical displacement of the overlying strata in the middle of the goaf was great larger than that of the overlying strata on both sides. Meanwhile, the maximum displacement point moved forward with the advance of the workface and constantly closed to the middle of the goaf. In addition, the vertical displacement of the overlying strata above the coal pillar at the same advancing distance of the workface increased with the increase of the distance from the workface, which was opposite to the vertical displacement of the overlying strata above the goaf. Moreover, the vertical displacement of overlying strata at the same location above the coal pillar gradually increased with the advance of the workface.

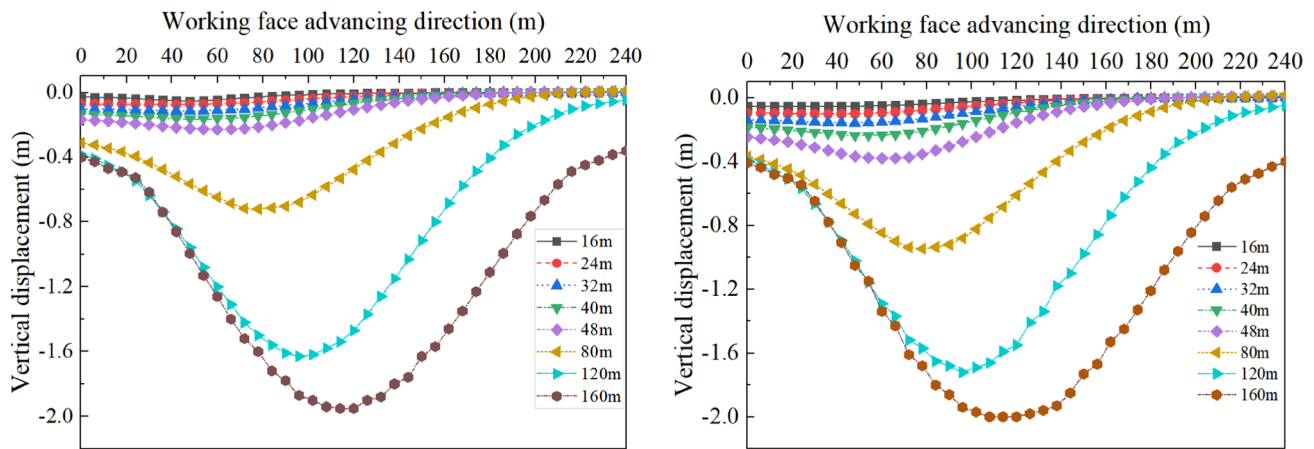
As shown in Fig. 22, the change of the displacement of overlying strata curve before 11 m from the workface in CI condition was basically the same, and the vertical



**Fig. 22** Vertical displacement curves of different layers with the advancing of workface (*left* was CI, *right* was CII). **a** Away from the workface 2.5 m. **b** Away from the workface 11 m. **c** Away from the workface 35 m. **d** Away from the workface 85 m

displacement curve was firstly transformed from “V” to “funnel”. It can be explained that the vertical displacement of the roof in the middle of the goaf was much larger than that of the roof on both sides of the goaf before the first

weighting pressure. Subsequently, the roof was broken periodically, and the maximum displacement value was basically unchanged. When the workface advancing to 40 m, the vertical displacement value had reached the peak value. However,



(d) Away from the workface 85 m

Fig. 22 (continued)

the vertical displacement of overlying strata away from the

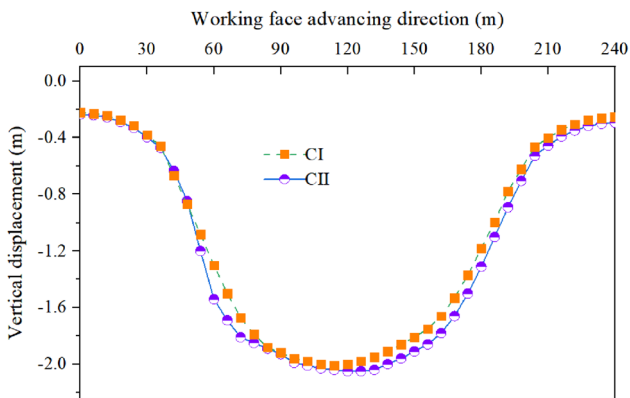


**Fig. 23** Vertical displacement curves of the top of aquiclude in CI and CII conditions

workface 35 m increased with the advance of the workface, while the change rate was small and uniform.

When the workface advancing from 24 to 32 m, the vertical displacement of the roof away from the workface 2.5 m increased sharply due to the occurrence of the initial weighting pressure and the broken of the main roof. This process was 8 m smaller than the advancing distance in the aquifer without water. When the working face advances to 40 m, the vertical displacement value of the roof at 11 m from the working face increases slowly. When the workface advancing to 48 m, the vertical displacement of the roof increased sharply, indicating that the rock stratum below the aquiclude was broken resulting in a sudden change in displacement. The vertical displacement of overlying strata away from the workface 35 m increased uniformly with the continuous advancement of the workface.

Figure 23 illustrated the vertical displacement of the top of the aquiclude in CI and CII conditions when the workface advancing to 160 m. It shown that the maximum displacement of both conditions was equal, and the point was located in the middle of the goaf. However, the subsidence of the top of the aquiclude in CII condition was more significant than that of CI conditions in the range of 50–90 and 130–180 m along the strike direction. When the working face advanced a certain distance, the upper rock strata in the middle of the goaf were basically stable with a compacted state, while the upper rock strata on the side of the open-off cut and the side of the workface were not fully collapsed with many separation spaces, as shown in Fig. 11d. Under the action of water seepage and water pressure, the separation space can be continuously compressed and closed. Therefore, within 50–90 and 130–180 m, the subsidence at the top of the water-bearing state was always larger than that of the non-water-bearing state.

## 6 Conclusion

In this paper, comprehensive analysis methods combining theoretical analysis, physical simulation and numerical simulation are used to comprehensively explain the failure mechanism and movement characteristics of overlying strata under the hydraulic coupling the thick aquifer. The expression of the initial and periodic breaking distance of aquiclude under hydraulic coupling is proposed. In addition, a physical similar simulation experiment under the combined action of pore-water pressure and water seepage is designed to explore the movement and deformation characteristics of overlying strata. Moreover, numerical simulation models



are constructed to further explore the effect of fluid–solid coupling mining in a thick aquifer on the failure mechanism and movement characteristics of overlying strata. The main conclusions are drawn as follows.

1. The initial and periodic breaking distance of the aquifuge increase with the increase of tensile strength of rock, and decrease with the increase of water head height, when mining activities under a thick aquifer condition,. In addition, the height of the water head is the main controlling factor for the breaking time and breaking position of the aquiclude.
2. The failure of overlying strata mining under thick aquifer is mainly characterized by tensile-bending breaking. The subsidence of overlying strata near the mining area is the largest, and the overlying strata above the goaf generally sink downward in a funnel shape. In addition, the combined effect of water seepage and water pressure is the main reason for the sudden change of fracture propagation velocity and roof subsidence velocity.
3. The pore-water pressure and water seepage under the thick aquifer have a significant effect on the failure and movement of the overlying strata, especially on the initial weighting distance of the main roof, the breaking distance of the aquiclude, the caving angle of the overlying strata, the distribution of the three zones of the overlying strata, and the subsidence on both sides of the goaf. Under the action of water pressure in thick aquifer, the initial weighting distance of the main roof and initial breaking distance of the aquifuge are significantly reduced.
4. The height of the caving zone and water-conducting fractured zone of the numerical simulation and the physical similarity simulation are basically the same, and the results of the two are slightly higher than the calculation results of the empirical formula, which is beneficial to the prevention of roof water inrush. In addition, the initial and periodic breaking distance of the aquifuge obtained by the two research methods are close to the calculation results of the theoretical model, and the periodic breaking distance of the aquifuge is about half of the initial breaking distance, which further verifies the calculation results of the theoretical model.

The fracture of rock strata under hydraulic coupling is a very complex process. The theoretical analysis in this paper is a simplified model based on material mechanics. In fact, the real structure of rock strata is quite complex, such as the uncertainty and irregular distribution of faults, pores, and joints in rock strata. Therefore, it is of great significant to further study the distribution law of faults, pores, and

joints under hydraulic coupling and the failure mechanism and characteristics of overlying strata under their irregular distribution. In addition, the mechanism and law of fracture propagation under hydraulic coupling will be also explored in future work.

**Acknowledgements** We acknowledge the financial support from the Guizhou Provincial Basic Research Program (Natural Science) (Qianke He Foundation-ZK [2024] Key 022), the Qianke He Platform Talents (GCC [2023] 056), Guizhou Provincial Department of Education 2023 Annual College Science and Technology Innovation Team (Guizhou Education Technology [2023] 055), National Natural Science Foundation of China Regional Fund (No. 52064005, 52164005, 52164002) and Guizhou University Cultivation Plan ([2020] No. 23).

**Funding** National Natural Science Foundation of China Regional Fund (No. 52164005, 52064005, 52164002), Guizhou Provincial Basic Research Program (Natural Science) (Qianke He Foundation-ZK [2024] Key 022), Qianke He Platform Talents (GCC [2023] 056), Guizhou Provincial Department of Education 2023 Annual College Science and Technology Innovation Team (Guizhou Education Technology [2023] 055), Guizhou University Cultivation Plan ([2020] No. 23).

**Data Availability** All data, models, and code generated or used during the study appear in the published article.

## Declarations

**Conflict of Interest** The authors declare that they have no known competing financial interests or personal relationships that could have appeared to influence the work reported in this paper.

## References

- Buddhima I, Mairaj HAAS, Cholachat R (2021) Semi-empirical analytical modelling of equivalent dynamic shear strength (EDSS) of rock joint. *Transp Geotech*:100569. <https://doi.org/10.1016/j.trgeo.2021.100569>
- Chen Y, Zhao G, Wang S, Wu H, Wang S (2019) A case study on the height of a water-flow fracture zone above undersea mining: Sanshandao Gold Mine, China. *Environ Earth Sci* 78(4). <https://doi.org/10.1007/s12665-019-8121-7>
- Chen L, Ou Q, Peng Z, Wang Y, Chen Y, Tian Y (2022) Numerical simulation of abnormal roof water-inrush mechanism in mining under unconsolidated aquifer based on overburden dynamic damage. *Eng Fail Anal* 133. <https://doi.org/10.1016/j.engfailanal.2021.106005>
- Ding J, Dong DL, Hu ZQ, Ji Y, Wei ZL (2022) Numerical simulations of how staged dewatering and mining influence surface subsidence. *Mine Water Environ* 41(4):1124–1136. <https://doi.org/10.1007/s10230-022-00903-5>
- Fan G, Zhang D (2015) Mechanisms of aquifer protection in underground coal mining. *Mine Water Environ* 34(1):95–104. <https://doi.org/10.1007/s10230-014-0298-0>
- Fan H, Zhu Z, Song Y, Zhang S, Zhu Y, Gao X, Hu Z, Guo J, Han Z (2021) Water pressure evolution and structural failure characteristics of tunnel lining under hydrodynamic pressure. *Eng Fail Anal* 130. <https://doi.org/10.1016/j.engfailanal.2021.105747>
- Feng G, Wang X, Kang Y, Zhang Z (2020) Effect of thermal cycling dependent cracks on physical and mechanical properties of

- granite for enhanced geothermal system. *Int J Rock Mech Min Sci*. <https://doi.org/10.1016/j.ijrmms.2020.104476>
- Gee D, Bateson L, Grebby S et al (2020) Modelling groundwater rebound in recently abandoned coalfields using DInSAR. *Remote Sens Environ* 249. <https://doi.org/10.1016/j.rse.2020.112021>
- Huang W, Li C, Zhang L et al (2018) In situ identification of water-permeable fractured zone in overlying composite strata. *Int J Rock Mech Min Sci* 105:85–97. <https://doi.org/10.1016/j.ijrmms.2018.03.013>
- Huang Z, Zhao K, Li X, Zhong W, Wu Y (2021) Numerical characterization of groundwater flow and fracture-induced water inrush in tunnels. *Tunn Under Sp Tech* 116. <https://doi.org/10.1016/j.tust.2021.104119>
- Kang JR, Wang JZ (2002) Mechanical model of the overburden rock under mining and the broken condition analysis. *J China Coal Soc* 27(1):16–20. <https://doi.org/10.13225/j.cnki.jccs.2002.01.004>
- Kong DZ, Li Q, Wu GY, Song GF (2021a) Characteristics and control technology of face-end roof leaks subjected to repeated mining in close-distance coal seams. *Bull Eng Geol Environ* 80(11):8363–8383. <https://doi.org/10.1007/s10064-021-02438-5>
- Kong DZ, Xiong Y, Cheng ZB, Wang N, Wu GY, Liu Y (2021b) Stability analysis of coal face based on coal face-support-roof system in steeply inclined coal seam. *Geomech Eng* 25(3):233–243. <https://doi.org/10.12989/gae.2021.25.3.233>
- Kong L, Ranjith PG, Li BQ (2021c) Fluid-driven micro-cracking behaviour of crystalline rock using a coupled hydro-grain-based discrete element method. *Int J Rock Mech Min Sci* 144:13651609. <https://doi.org/10.1016/j.ijrmms.2021.104766>
- Li SC, Wu J, Xu ZH, Yang W M (2019) Mechanics criterion of water inrush from the coal floor under influence of fault and its engineering application. *Int J Geomech* 19(5). [https://doi.org/10.1061/\(asce\)gm.1943-5622.0001387](https://doi.org/10.1061/(asce)gm.1943-5622.0001387)
- Li C, Zuo J, Xing S, Du W, Chuai X (2022) Failure behavior and dynamic monitoring of floor crack structures under high confined water pressure in deep coal mining: a case study of Hebei, China. *Eng Fail Anal* 139. <https://doi.org/10.1016/j.engfailanal.2022.106460>
- Liu J, Elsworth D (1997) Three-dimensional effects of hydraulic conductivity enhancement and desaturation around mined panels. *Int J Rock Mech Min Sci* 34(8):1139–1152. [https://doi.org/10.1016/S1365-1609\(97\)80067-6](https://doi.org/10.1016/S1365-1609(97)80067-6)
- Mairaj HAAS, Buddhima I, Shivakumar K (2022) Critical shear strain and sliding potential of rock joint under cyclic loading. *Transp Geotech* 32. <https://doi.org/10.1016/j.trgeo.2021.100708>
- Manzano M, Ayora C, Domenech C, Navarrete P, Garralon A, Turrero MJ (1999) The impact of the Aznalcollar mine tailing spill on groundwater. *Sci Total Environ* 242(1–3):189–209. [https://doi.org/10.1016/S0048-9697\(99\)00384-8](https://doi.org/10.1016/S0048-9697(99)00384-8)
- Manhong X, Shaogang D, Yue C et al (2021) Study on evolution of groundwater-lake system in typical prairie open-pit coal mine area. *Environ Geochem Hlth* 43(10):4075–4087. <https://doi.org/10.1007/s10653-021-00890-6>
- Meng Z, Li G, Xie X (2012) A geological assessment method of floor water inrush risk and its application. *Eng Geol* 143:51–60. <https://doi.org/10.1016/j.enggeo.2012.06.004>
- Meng Z, Shi X, Li G (2016) Deformation, failure and permeability of coal-bearing strata during longwall mining. *Eng Geol* 208:69–80. <https://doi.org/10.1016/j.enggeo.2016.04.029>
- Miao X, Cui X, Wang J et al (2011) The height of fractured water-conducting zone in undermined rock strata. *Eng Geol* 120(1):32–39. <https://doi.org/10.1016/j.enggeo.2011.03.009>
- Niu XH, Feng GR, Liu Q, Han YN, Qian RP (2022) Numerical investigation on mechanism and fluid flow behavior of goaf water inrush: a case study of Dongyu coal mine. *Nat Hazards* 113(3):1783–1802. <https://doi.org/10.1007/s11069-022-05369-w>
- Pathan SM, Pathan AG, Siddiqui FI, Memon MB, Soomro MHAA (2022) Open pit slope stability analysis in soft rock formations. *Arch Min Sci* 3(67):437–454. <https://doi.org/10.24425/ams.2022.142409>
- Rui G, Hao Y, Feng J, Mei X, Wang X (2018) Influential factors and control of water inrush in a coal seam as the main aquifer. *Int J Min Sci Techno* 28(2):187–193. <https://doi.org/10.1016/j.ijmst.2017.12.017>
- Shang YQ, Kong DZ, Pu SJ, Xiong Y, Li Q, Cheng ZB (2022) Study on failure characteristics and control technology of roadway surrounding rock under repeated mining in close-distance coal seam. *Mathematics* 10(13). <https://doi.org/10.3390/math10132166>
- Shi ZD, Han YX (1987) Course of elastic mechanics [M]. Bei Hang University Press, Beijing
- Song W, Jian Z, Luqing Z et al (2023) Modeling injection-induced fracture propagation in crystalline rocks by a fluid-solid coupling grain-based model. *Rock Mech Rock Eng* 56(8):5781–5814. <https://doi.org/10.1007/s00603-023-03374-4>
- Sun J, Hu Y, Zhao G (2017) Relationship between water inrush from coal seam floors and main roof weighting. *Int J Min Sci Techno* 27(5):873–881. <https://doi.org/10.1016/j.ijmst.2017.07.010>
- Sun Q, Zhang JX, Zhou N, Huang YL (2021) Key Aquiclude strata reconstruction and fluid-solid coupled deformation mechanism study for backfill coal mining. *Mine Water Environ* 40(3):793–802. <https://doi.org/10.1007/s10230-021-00786-y>
- Sikora P, Wesołowski M (2021) Numerical assessment of the influence of former mining activities and plasticity of rock mass on deformations of terrain surface. *Int J Min Sci Technol* 31(2):209–214. <https://doi.org/10.1016/j.ijmst.2020.11.001>
- Wang J, Tang J, Jiao S (2015) Seepage prevention of mining-disturbed riverbed. *Int J Rock Mech Min Sci* 75:1–14. <https://doi.org/10.1016/j.ijrmms.2014.10.010>
- Wang X, Xu ZM, Sun YJ, Zheng JM, Zhang CH, Duan ZW (2021a) Construction of multi-factor identification model for real-time monitoring and early warning of mine water inrush. *Int J Min Sci Technol* 31(5):853–866. <https://doi.org/10.1016/j.ijmst.2021.07.012>
- Wang XH, Zhu SY, Yu HT, Liu YX (2021b) Comprehensive analysis control effect of faults on the height of fractured water-conducting zone in longwall mining. *Nat Hazards* 108:2143–2165. <https://doi.org/10.1007/s11069-021-04772-z>
- Wang YL, Wu GY, Liu Y, Cheng ZB (2022) Study on overlying strata movement and surface subsidence of coal workfaces with karst aquifer water. *Mathematics* 10(2). <https://doi.org/10.3390/math10020169>
- Wu J, Jia C, Zhang LW (2021) Expansion of water inrush channel by water erosion and seepage force. *Int J Geomech* 21(7). [https://doi.org/10.1061/\(asce\)gm.1943-5622.0001985](https://doi.org/10.1061/(asce)gm.1943-5622.0001985)
- Yang T, Liu J, Zhu W (2007) A coupled flow-stress-damage model for groundwater outbursts from an underlying aquifer into mining excavations. *Int J Rock Mech Min Sci* 44(1):87–97. <https://doi.org/10.1016/j.ijrmms.2006.04.012>
- Yi LP, Waisman H, Yang ZZ, Li XG (2020) A consistent phase field model for hydraulic fracture propagation in poroelastic media. *Comput Method Appl Mech Eng* 372:113396. <https://doi.org/10.1016/j.cma.2020.113396>
- Zhang J, Shen B (2003) Coal mining under aquifers in China: a case study. *Int J Rock Mech Min Sci* 41(4):629–639. <https://doi.org/10.1016/j.ijrmms.2003.01.005>

- Zhang J, Peng S (2005) Water inrush and environmental impact of shallow seam mining. *Environ Geol* 48(8):1068–1076. <https://doi.org/10.1007/s00254-005-0045-8>
- Zhang D, Fan G, Liu Y, Ma L (2010) Field trials of aquifer protection in longwall mining of shallow coal seams in China. *Int J Rock Mech Min Sci* 47(6):908–914. <https://doi.org/10.1016/j.ijrmms.2010.06.018>
- Zhang T, Gan Q, Zhao Y et al (2019) Investigations into mining-induced stress-fracture-seepage field coupling effect considering the response of key stratum and composite aquifer. *Rock Mech Rock Eng* 52(10):4017–4031. <https://doi.org/10.1007/s00603-019-01811-x>
- Zhang H, Xu G, Zhan H et al (2020) Identification of hydrogeochemical processes and transport paths of a multi-aquifer system in closed mining regions. *J Hydrol* 589. <https://doi.org/10.1016/j.jhydrol.2020.125344>
- Zhao C, Liu J, Lyu C, Xu D, Liang C, Li Z (2022) Investigation on the mechanical behavior, permeability and failure modes of limestone rock under stress-seepage coupling. *Eng Fail Anal* 140. <https://doi.org/10.1016/j.engfailanal.2022.106544>

**Publisher's Note** Springer Nature remains neutral with regard to jurisdictional claims in published maps and institutional affiliations.

Springer Nature or its licensor (e.g. a society or other partner) holds exclusive rights to this article under a publishing agreement with the author(s) or other rightsholder(s); author self-archiving of the accepted manuscript version of this article is solely governed by the terms of such publishing agreement and applicable law.